

Turbulence, Acoustic Backscatter and Pelagic Nekton in Monterey Bay

MICHAEL C. GREGG *

APPLIED PHYSICS LABORATORY, UNIV. OF WASHINGTON, SEATTLE, WA

JOHN K. HORNE

SCHOOL OF AQUATIC AND FISHERY SCIENCES, UNIV. OF WASHINGTON, SEATTLE, WA

* *Corresponding author address:* M. C. Gregg, Applied Physics Lab. & School of Oceanography, Box 355640, Univ. Washington, Seattle, WA 98105.

E-mail: gregg@apl.washington.edu

ABSTRACT

During August 2006 several aggregations of nekton, most likely small fish, intersected microstructure survey lines in Monterey Bay, California, providing an opportunity to examine biologically-generated mixing. Some aggregations filled the water column, 80 m deep, and extended 100–200 m along the survey track. Others were half that size, and some were much smaller. Acoustic energy backscattered from the aggregations was measured with a calibrated echosounder and yielded -80 to -60 dB re 1 m^{-1} for the volume backscattering strength, S_v .

Turbulent dissipation rates, ϵ , were 10^{-6} to $10^{-5} \text{ W kg}^{-1}$ in the more intense aggregations. Within these, ϵ was much more uniform than turbulence measured outside the aggregations and varied with S_v . Three similar aggregations contributed half of the average ϵ in 142 profiles taken along a 5-km-long survey line during a 12.5-h tidal cycle.

Turbulence within aggregations differed markedly from that outside. Specifically: a) Thorpe scales, i.e., root-mean-square overturning lengths, were much smaller than Ozmidov scales, $L_{OZ} \equiv (\epsilon/N^3)^{1/2}$, the upper limit for overturns limited by stratification. b) Spectra of small-scale shear matched the universal shape only in the viscous high-wavenumber rolloff. At lower wavenumbers, the shear spectra had slopes closer to k^1 than to the $k^{1/3}$ Kolmogorov slope. Consequently, the corresponding velocity spectra peaked near 0.08 cpm. c) Temperature gradient spectra matched portions of the universal Batchelor spectrum that could be resolved, but their magnitudes were much smaller than those in turbulence produced by flow instabilities. As a result, the average mixing efficiency, Γ , was

0.0022 within aggregations, compared with 0.23 outside. This 100-fold decrease in efficiency compensates for a 100-fold increase in ϵ to produce no net change in diapycnal diffusivity, K_ρ . Because we are uncertain of the composition of the aggregations and of the behavior, i.e., whether the nekton had the regular spacing and swimming patterns characterizing schools, it is not possible to know whether we sampled only one turbulent state or many of those possible in aggregations. If these observations are representative, mixing in aggregations may be more interesting than it is important, but the data are too few for definitive conclusions.

1. Introduction

During August 2006 a mixing survey of Monterey Bay encountered aggregations of nekton, probably fish, along several survey lines, allowing us to examine predictions that biologically-generated turbulence is an important agent mixing the ocean. Microstructure profiles penetrated some of the aggregations providing estimates of viscous and thermal dissipation rates, ϵ and χ_T , as well as overturning scales to quantify biologically-generated mixing and its efficiency. Simultaneous backscatter of narrow-beam high-frequency pulses allowed some characterization of the aggregations, but, without net tows, their composition remained uncertain. After summarizing relevant background in section 2, acoustic characteristics of the aggregations are examined in section 3 to infer as much as possible about the size, density, and constituents of the aggregations. Dissipation rates are compared with acoustic intensity and with dissipation in background turbulence in section 4. Spectra and overturning scales are presented in section 5 to characterize the nature of the turbulence, information used in section 6 to calculate mixing efficiencies, which are required to estimate the net effect of the turbulence in terms of turbulent diffusivity. Results are summarized and discussed in section 7. Observational details are included in the appendix.

2. Background

Roughly parallel developments of microstructure instruments and of high-frequency acoustic backscatter systems deployed in the ocean have produced a large and growing literature identifying biological and turbulent sources of echo sounder signals and, more recently, es-

timating the role of biological mixing in the ocean. Biologically-generated mixing is one of the possibilities Munk (1966) listed as alternatives to mixing produced by breaking internal waves.

Farmer et al. (1987) briefly noted sharp increases in ϵ and χ_T in horizontal transects through a nekton aggregation found in a mixed layer in Monterey Bay. More recently, while profiling in Saanich Inlet, British Columbia, Kunze et al. (2006) discovered that as krill ascended during dusk, ϵ increased by an astonishing four decades, from 10^{-9} to 10^{-5} W kg^{-1} . Not all evening ascents produced intense turbulence, but those that did raised the daily average diapycnal diffusivity, K_ρ , to $4 - 40 \times 10^{-4}$ $\text{m}^2 \text{s}^{-1}$ compared with 2×10^{-6} $\text{m}^2 \text{s}^{-1}$ when those data were omitted. The diffusivity was estimated using

$$K_\rho = \Gamma \frac{\epsilon}{N^2} \quad (1)$$

where Γ is the mixing efficiency. Following standard practice, Kunze et al. used $\Gamma = 0.2$ (Osborn 1980). In view of the large increase in K_ρ , Kunze et al. suggest that the mixing produced by krill migrations may have global significance.

In response to Kunze et al. (2006), Rippeth et al. (2007) re-examined 11 sets of profiles in coastal waters west of the British Isles. No significant increase in ϵ was found during times of vertical migrations, demonstrating that strong mixing during vertical migrations cannot be assumed in all coastal waters. As noted by Kunze and Dower (2007), because Rippeth et al. lacked information about the species and densities of migrating organisms it is not possible to compare their results directly with those from Saanich Inlet, and more observations are needed to determine how species and abundance affect turbulence accompanying vertical migrations.

Dewar et al. (2006) estimate that 1% of the 62.7 TW primary production in the ocean produces mixing, a rate comparable to that resulting from tides and winds. They infer that ≈ 1 TW occurs below the euphotic zone. Assuming $\Gamma = 0.2$ and distributing the 1 TW over the upper 3 km gives $K_\rho \approx 2 \times 10^{-5} \text{ m}^2 \text{ s}^{-1}$, somewhat larger than that observed above the thermocline, where the mixing has been attributed to breaking internal waves (Garrett and Munk 1975).

Visser (2007) disagrees with these estimates, arguing that organisms cannot generate overturning scales larger than themselves. Although they may generate large ϵ , owing to the reduced overturning scales, Γ must be closer to 10^{-4} – 10^{-2} than to the 0.2 characterizing turbulence generated by flow instabilities. Using Richardson’s law (Richardson 1926) to represent K_ρ , Visser obtained $\Gamma = (L_{\text{TH}}/L_{\text{OZ}})^{4/3}$. The Ozmidov scale, $L_{\text{OZ}} \equiv (\epsilon/N^3)^{1/2}$, is the vertical interval over which stratification limits turbulent overturns. Here, we represent Visser’s overturning scale, l , by L_{TH} , the rms overturning scale determined by comparing observed and monotonically increasing density profiles (Thorpe 1977).

In contrast to these general arguments, Huntley and Zhou (2004) took a ‘tail-up’ approach to biologically induced mixing by analyzing the hydrodynamic characteristics of marine animals. They began with the work done by a single swimmer to overcome drag, $e_d = u_c D$ [W], where u_c is the cruising speed and D the drag. The expression used for drag is: $D = (1/2)\rho C_d A_w u_c^2$ [N], where $C_d = 0.072 Re^{-0.2}$ is the drag coefficient for a flat plate, and $A_w = (1/2)WL$ is the wetted area with W the width and L the length of the animal. The total rate of energy expended by a group of animals in a school with fairly regular spacing

between animals of the same species is

$$E_p = \frac{e_d N_f}{\rho \eta V} = \frac{1.34 \times 10^{-5} M^{1.39} N_f}{\eta V} \quad [\text{W kg}^{-1}] \quad (2)$$

where η is the efficiency of the swimmers and N_f/V their number per unit volume. Simple power-law expressions for u_c and the Reynolds number in terms of body mass, M , allow evaluating energy expended for different species. As an example, for the northern anchovy (*Engraulis mordax*) $M = 0.010$ kg, $u_c = 0.14$ m s⁻¹, $\eta = 0.24$, and $N_f/V = 115$ m⁻³ yielding $E_p = 1.06 \times 10^{-5}$ W kg⁻¹, which is ϵ in the water. Huntley and Zhou (2004) further assume that the maximum packing density within aggregations is inversely related to body mass, obtaining $N_f/V = 0.64M^{-1.2}$. As a result, they predict that dissipation rates in schools are approximately 10^{-5} W kg⁻¹, regardless of whether the animals are whales or zooplankton.

Taking an observational approach using two-dimensional particle velocimetry, Muller et al. (1997) observed the wake of a juvenile mullet, 0.12 m long, swimming continuously in a tank. The wake consisted of vortex rings, two per tailbeat cycle, and a jet between the vortices. The wake was an inverse von Karman vortex train, i.e., the vortices had opposite signs, and their average power was 0.56 mW. There was no information about schooling behavior of mullets, but $N_f/V = 100$ would give an average dissipation of $\epsilon = 5.6 \times 10^{-4} \times 10^2/\rho = 5.6 \times 10^{-5}$ W kg⁻¹. Videler et al. (2002) provided more details: maximum vorticity was 20 s⁻¹ in the center of the vortex closest to the fish, and maximum velocity was 91 mm s⁻¹, in the second vortex from the tail. The width of the wake was about 80 mm.

Simulating a swimming fish using a three-dimensional hydrodynamics model, Cheng and Chahine (2001) conclude that ‘undulatory’ swimming reduces three-dimensional effects due

to substantially weakened tail vortices, resulting in a reverse Karman vortex street. Flow around the fish is dominantly two-dimensional, and the vortices shed from its tail are nearly vertical when the fish swims horizontally.

3. Acoustic Characterization of Aggregation Backscatter

Because tidal currents produce or affect most mixing in shallow water, we surveyed mixing in Monterey Bay by repeating slow, $\approx 1 \text{ m s}^{-1}$, transects along survey lines for 12.5 h, the period of the twice-daily tide. Each set of transects was termed a group, and the individual runs were labeled subs. On average, a cast with one of our Modular Microstructure Profilers (MMPs, described in the appendix) was taken every 4.6 min. For comparison, the buoyancy period was 5–15 min.

Contours of the logarithm of the turbulent dissipation rate revealed columns of intense turbulence decades larger than in adjacent profiles in some subs (Fig. 1), leading us to suspect that the airfoils measuring the turbulence had been temporarily fouled. ADCP profiles, however, had simultaneous anomalies, in this case westward with $u \approx -0.1 \text{ m s}^{-1}$ against a generally eastward flow. Unique signatures were also found in the intensity of backscattered high-frequency sound from a scientific echo sounder (also discussed in the appendix). Backscatter patterns during Group 2 along the same track are similar to those observed by bioacousticians studying nekton aggregations (Fig. 2). These examples are representative of the large aggregations we found, but, lacking three-dimensional surveys,

we cannot be certain that we sampled three different aggregations rather than resampled the same one after its acoustic shape evolved. Two hundred meters across at the top and half that at the bottom, the aggregation sampled during Group 2, Sub 6 (panel A) nearly filled the water column. S_v was most intense above 50 m, particularly toward the right in the plot, and decreased 20 dB re 1 m^{-1} with depth, especially toward the left, before increasing again in the bottom 20 m. The aggregation during Group 2, Sub 7 (panel B) was largest at the bottom and S_v was more variable, a pattern repeated in Group 2, Sub 8 (panel C). Finally, a cluster of three medium-sized aggregations was found in the northwest part of the bay by Group 14, Sub 1 (panel D). The last of this trio filled half of the water column and extended laterally 100 m. S_v was largest in the middle of the three aggregations and moderate in the last.

Aggregation Characteristics

Ten aggregations were penetrated by an MMP during Group 2, which began at 0251 and ended at 1152 PDT 10 August. Aggregations detected at a $-65 \text{ dB re } 1 \text{ m}^{-1}$ threshold (Table 1) were elongated vertically with backscatter intensities increasing from the peripheries to the centroids of the aggregations. Table 2 reports descriptive metrics from the sampled aggregations. Using average depth as an index, aggregations generally occupied the lower half of the 80–85-m-deep water column and ranged in average height from 5.4 to 41.4 m. Aggregation chord lengths, $\overline{\Delta x}$, spanned an order of magnitude (i.e., from 26 to 190 m), while vertical thickness ranged from 11 m (14919) to the entire water column (15017). Based on speeds of the aggregations observed with the *Revelle* hydrographic ship sonar, errors in

horizontal size were estimated to be no more than 10–20%.

Acoustic Properties

Average volume backscattering strengths (i.e., mean Sv in units of dB re 1 m⁻¹) of aggregations in Group 2 ranged from -60.7 to -41.5 dB re 1 m⁻¹. Backscatter intensities increased at one or more focal points located in the interior of aggregations. Estimates of numeric or biomass densities of ensonified schools depend on transect location through aggregations (i.e., chord length), backscatter intensity, and assumed identity of constituents. No effort was made to map aggregation boundaries during MMP profiling, and it was assumed that all transects bisecting aggregations had equal probabilities of occurrence. It is also assumed that observed backscatter intensities were proportional to nekton densities (Foote 1983). At the -65 dB re 1 m⁻¹ threshold used to detect aggregations, there was evidence of potential acoustic shadowing for aggregations 15009, 15041, 15045, and 15057. Without in situ biological sampling and multiple acoustic frequencies, there is no definitive way to confirm the identity of organisms within aggregations. The most likely candidates comprising observed aggregations in Monterey Bay are large zooplankton or small fish. The two dominant krill species are Pacific krill (*Euphausid pacifica*) and *Thysanoessa spinifera*. Pacific krill are 22–25 mm long (Boden et al. 1955), reside below the continental shelf in horizontal layers during the day, and migrate to near surface waters at night (Fiedler et al. 1998). *Thysanoessa spinifera*, 20–38 mm long (Boden et al. 1955), are found in shallower waters and also disperse during dark hours (Schoenherr 1991; Croll et al. 2005). Small fish species found in Monterey Bay include northern anchovy (*Engraulius mordax*) and sardine (*Sardinops sagax caerule*).

Anchovy and sardine are dominant, pelagic species in the California Current ecosystem and have been examined acoustically since the 1970s (Smith 1970; Hewitt et al. 1976). The shape and contiguity of the observed aggregations suggest that the constituents were fish.

If all acoustic backscatter originated from 0.12-m anchovies weighing 0.013 kg (Mais 1974; Conti and Demer 2003) with average target strengths of 44.5 dB re 1 m⁻¹, then the density of targets along the track was $N_f = S_v / \sigma_{\text{BS}}^{\text{anchovy}}$, where $\sigma_{\text{BS}}^{\text{anchovy}}$ is the backscatter cross-section for anchovies. Combining N_f with volumes of the aggregations determined from the acoustics yields the number per unit volume (Table 2). As a consistency check on our assumptions, the correlation coefficient between N_f/V and S_v is $R = 0.80$, with negligible chance this occurred randomly.

The highest average backscatter, in aggregation 15045, resulted in estimated numeric and biomass densities at least double those of any other observed aggregation. Average numeric density among observed aggregations exceeded 3 million fish per square nautical mile with a corresponding mass density of over 40 thousand kg per square nautical mile. If all backscatter was produced by sardines instead of anchovies, then, using analogous anchovy and sardine species from the Benguela Current, target strengths would be approximately 5 dB kg⁻¹ larger (Barange et al. 1996) and numeric and mass density estimates would be correspondingly smaller.

4. Acoustic Intensity and Dissipation in the Backscatter Aggregations

Figure 3 typifies the background stratification. A strong pycnocline extended to 0.25 MPa, below which several weakly stratified layers were separated by strong steps. The layer at 60 m was well mixed in the mean and at the center of a large cloud of particulates extending from 45 to 75 m, which were not related to the aggregation. Assuming isotropy, the dissipation rates were computed as $\epsilon = 75\nu\overline{(\partial u'/\partial z)^2}$, where ν is the kinematic viscosity. In this and many other profiles of Sub 2 not in aggregations, ϵ rose above the general background level of $\approx 10^{-9}$ W kg $^{-1}$ in patches where $10^{-8} \leq \epsilon \leq 10^{-7}$, in some cases extending vertically for several tens of meters.

Figures 4–7 summarize MMP profiles through the aggregations represented in Fig. 2(A–D). The first three aggregations had dissipation rates, ϵ , 10 to 100 times maximum rates outside aggregations. Several aggregations maintained these elevated rates over tens of meters vertically, compared with 10 m or less in background mixing regions. For example, compare the background patch centered near 60 m in MMP 15018 (Fig. 3) with dissipation in the aggregation sampled by MMP 15017 (Fig. 4). Dissipation in the background patch peaked at 10^{-7} W kg $^{-1}$ and exceeded 10^{-8} over a 10-m interval. In marked contrast, in the aggregation $10^{-6} \leq \epsilon \leq 10^{-4}$ W kg $^{-1}$ between 30 and 60 m. Turbulent intensity, measured using the buoyancy Reynolds number, $Re_B \equiv \epsilon/\nu N^2$, was 10^4 – 10^5 in large aggregations. Gargett et al. (1984) found that as turbulence decayed some departures from isotropy appeared around $Re_B \approx 200$, but they noted that their results applied only to turbulence following buoyancy scaling. Dissipation was not as intense in the last cluster of moderate-

size aggregations (Fig. 7), but nevertheless stood out from the background (Fig. 2D).

The strong correlation of ϵ with S_v in Figs. 4 and 7 is striking. For MMP 15017, the correlation coefficient between S_v and $\log_{10} \epsilon$ is $R = 0.74$ with 95% confidence limits of 0.61 and 0.83. For MMP 17259, the correlation coefficient is essentially the same, $R = 0.73$. As expected, correlations between S_v and $\log_{10}(\epsilon)$ for background profiles did not differ significantly from zero. For MMP 15041, $R = 0.19$, significant but weakly correlated. As discussed below, it may be that the MMP trajectory is misleading and the profiler did not remain within the aggregation, passing through it only from 0.5 to 0.7 MPa.

5. Turbulent Spectra and Overturning Scales

To assess the effect of biological aggregations on mixing, it is first necessary to compare turbulence characteristics of aggregations with those of background mixing patches in the bay. Spectral characteristics are examined first, and then overturning scales are compared with those expected based on dissipation rates and stratification.

Turbulent Spectra

Only from the spectral peak to the high-wavenumber resolution limit of the airfoils do shear spectra in aggregations match the Panchev and Kesich (1969) universal spectrum for well-developed turbulence; ϵ , the only adjustable parameter, was obtained by integrating observed spectra assuming isotropy. At lower wavenumbers, spectral slopes are close to k^1 , falling well below the $k^{1/3}$ slope of the viscous, or Kolmogorov, subrange. Figure 8a is

an example from MMP 15017 and is representative of spectra of other profiles through aggregations. At 2 cpm the observed spectra are only 1/6 of the Panchev and Kesich spectrum, and the slope is close to k^1 . This discrepancy, however, has negligible effect on the distribution of variance in a variance-preserving plot.

The mismatch of observed and theoretical spectra in aggregations contrasts with observations in strong or moderate background turbulence (Gregg et al. 1996). For example, Fig. 9 shows a shear spectrum from the next MMP profile, which was outside the aggregation. From 0.5 to 0.65 MPa, dissipation was fairly homogeneous with $\bar{\epsilon} = 4.92 \times 10^{-8} \text{ W kg}^{-1}$, moderately strong for the thermocline. The lower wavenumbers remain close to the universal form, unlike those within intense aggregations.

Figures 10 and 11 display velocity spectra corresponding to the shear spectra in Figs. 8 and 9. The variance-preserving spectrum for MMP 15017 peaks at 8 cpm, corresponding to a length scale of 0.13 m. Integrating from 2 to 70 cpm yields an rms velocity of 0.4 mm s^{-1} for one component of horizontal velocity. In contrast, the variance-preserving spectrum for MMP 15018 follows the universal shape, with no peak at these length scales.

Temperature microstructure was measured during the first half of the observations, providing valuable information about mixing in the aggregations, but the temperature probes were removed during the second half to free data channels so oxygen probes could be recorded for tracking water masses. Because the FP07 thermistors used for microstructure were not calibrated dynamically, corrections for dynamic attenuation rely on a nominal time constant (see appendix for additional detail).

At MMP fall rates of $0.6\text{--}0.7 \text{ m s}^{-1}$, the FP07 thermistors did not resolve the temperature gradient spectrum within the intense aggregations. Consequently, we computed the

theoretical Batchelor spectrum using the observed ϵ and molecular diffusivities and adjusted its amplitude to obtain χ_T , the rate of diffusive destruction of turbulent temperature fluctuations. The only adjustable parameter in the Batchelor spectrum is χ_T , defined as

$$\chi_T \equiv 2\kappa_T \overline{(\nabla T')^2} = 2\kappa_T(1-3)\overline{(\partial T'/\partial z)^2} = 2\kappa_T C (\partial \bar{T}/\partial z)^2 \quad (3)$$

where κ_T is the molecular diffusivity of heat in water, and the factor $(1-3)$ is the degree of isotropy. Full isotropy, i.e., a factor of 3, has been assumed. In the alternate expression, C is the Cox number,

$$C \equiv \frac{\overline{(\nabla T')^2}}{(\partial \bar{T}/\partial z)^2} = \frac{(1-3)\overline{(\partial T'/\partial z)^2}}{(\partial \bar{T}/\partial z)^2} \quad (4)$$

Because the Cox number is a better measure of turbulent intensity than is χ_T , it is used below as a measure of spectral magnitude and is a key factor in estimates of mixing efficiency presented below.

To estimate the Cox number, temperature gradient spectra were computed over sections where the mean temperature profile was nearly linear. Figure 12 shows the temperature profile and gradient spectrum from a section within the aggregation sampled by MMP 15017. Up to the spectral peak, the observed spectrum is a good fit to the theoretical spectrum, yielding $C = 850$. A well-resolved spectrum outside an aggregation is shown in Fig. 13. Its magnitude corresponds to $C = 250$. Cox numbers for other spectra, within and outside aggregations, are given in Table 3.

Overtuning Scales

Overtuning scales were estimated in two ways. The buoyancy, or Ozmidov, scale characterizes the energy-containing scale of steady turbulence limited by stratification. It was

computed using N^2 , the square of the buoyancy frequency, obtained after density was sorted to increase monotonically. The sorted profile is a better estimate of the stratification that was overturned than is the observed stratification.

Thorpe scales, defined above, are the best available estimates of overturning scales. As first shown by Dillon (1982), Ozmidov and Thorpe scales for active overturns are approximately equal, $L_{\text{TH}} \approx 0.8L_{\text{OZ}}$ for averages, but with considerable scatter. Because the vertical resolution of our density data, collected with Sea-Bird CTDs on the MMPs, is too coarse to resolve energy-containing scales in these profiles, we used Thorpe scales computed from temperature sensed with FP07 thermistors in regions that appear free of salt-stabilized temperature inversions. For profiles of primary interest, this condition was obtained between 30 and 65 m (Fig. 14), with the boundaries varying slightly among profiles. Any errors resulting from using temperature instead of density overestimated Thorpe scales.

Outside aggregations, Thorpe and Ozmidov scales agreed well in profiles 15016 and 15017 (Fig. 15) except for a few cases where N^2 was very small in nearly homogeneous layers. In stark contrast, Thorpe scales were much less within aggregations. In particular, between 35 and 52 m of MMP 15017 the Thorpe scales varied slightly about 0.1 m, close to the peak of the variance-preserving velocity spectrum, while most of the Ozmidov scales exceeded 1 m. Comparing estimates of L_{OZ} and L_{TH} from many profiles (Fig. 16), there appear to be two slightly overlapping groups. Overturns outside aggregations scattered around $L_{\text{Th}} = L_{\text{OZ}}$ and were similar to earlier background observations (Dillon 1982). Overturns within aggregations had an L_{Th} centroid of about 0.05 m compared to 0.25 m for the corresponding L_{OZ} . Consequently, the energy-containing scales of turbulence within aggregations were much smaller than those for turbulence limited by stratification.

6. Mixing Efficiency and Diapycnal Diffusivity

Diapycnal turbulent diffusivities of heat vary directly with Cox numbers as

$$K_T = C\kappa_T \quad [\text{m}^2 \text{s}^{-1}] \quad (5)$$

(Osborn and Cox 1972). Hence, $C = 850$ from 36 to 42 m in MMP 15017 corresponds to $K_T = 1.21 \times 10^{-4} \text{ m}^2 \text{ s}^{-1}$.

Diapycnal diffusivity, K_ρ , is routinely estimated from measurements of small-scale shear using (1) with $\Gamma = 0.2$ (Osborn 1980). Thus, $\epsilon = 2.34 \times 10^{-6} \text{ W kg}^{-1}$ over the above interval yields $K_\rho = 9.2 \times 10^{-3} \text{ m}^2 \text{ s}^{-1}$, nearly 100 times K_T . Since Oakey (1982), mixing efficiency, Γ , has been estimated from simultaneous measurements of temperature and velocity microstructure by assuming that $K_\rho = K_T$, leading to

$$\Gamma = \kappa_T C N^2 / \epsilon \quad (6)$$

For example, Oakey (1982) obtained $\Gamma = 0.24$; Peters et al. (1988) found ≈ 0.1 in the equatorial undercurrent except at the core where $\Gamma \approx 0.2$; Gregg et al. (1986) obtained 0.18; and Moum (1996) found $\Gamma = 0.15 - 0.20$. None differ greatly from $\Gamma = 0.2$, assumed by Osborn (1980)

Estimates of Γ from Monterey Bay mirror the two groups found by comparing overturning scales: values within aggregations were much smaller than those outside (Table 3). For example, from 36 to 40 m in MMP 15017, $\Gamma = 0.0026$, a 100-fold reduction below the standard range, demonstrating that mixing within aggregations is much less efficient than mixing produced by background turbulence.

Continuing with MMP Group 2 as representative of Monterey Bay including the aggre-

gations, Fig. 17 displays the vertical group average of ϵ for the 142 profiles. The thick line is the group average, and the thin line is the average omitting data in major aggregations, i.e., removing portions of profiles 15017, 15041, and 15057. Averaged between 0.35 and 0.80 MPa, turbulence in the three aggregations accounted for half of the net dissipation measured during Group 2. Consequently, although ϵ in the aggregations was 100 times that outside, mixing efficiency was reduced by almost the same factor to produce nearly the same diapycnal diffusivity.

7. Summary and Discussion

Acoustic backscatter revealed large aggregations of nekton, i.e., organisms able to move independent of fluid motions, in Monterey Bay during August 2006. Lacking in situ biological samples, the species cannot be identified with certainty but were most likely anchovies or sardines. Similarly, without a suite of acoustic frequencies, it is not possible to determine whether the aggregations had the relatively regular spacing and behavior of schools. While we were measuring microstructure along survey lines, our profilers sampled turbulence and stratification in a few of the aggregations, allowing us to examine some of the current issues about biologically induced mixing and to reach several conclusions:

1. Within the largest aggregations, the acoustic volume backscattering strength, S_v , rose from noise levels of -120 dB re 1 m^{-1} to more than -80 dB re 1 m^{-1} at 120 and 208 kHz. The largest aggregations were 60–70 m in the vertical, nearly filling the water column, and extending laterally 50–200 m.

2. Average turbulent dissipation rates, ϵ , were 10^{-7} to 10^{-5} W kg^{-1} in aggregations, ten to one hundred times those in the more intense patches of background turbulence. In several cases, ϵ was strongly correlated with S_v .
3. Key turbulence characteristics of the large aggregations differed from those of background turbulence:
 - (a) Spectra of vertical shear matched the universal turbulent spectrum only in the viscous rolloff at high wavenumber. At wavenumbers smaller than the spectral peak, spectral slopes were closer to k^1 than to the $k^{1/3}$ Kolmogorov slope. As a consequence, variance-preserving velocity spectra had maxima at 0.08 cpm, corresponding to vertical length scales of 0.12 m, unlike the universal spectrum which does not peak in the dissipation range.
 - (b) Thorpe scales, i.e., root-mean-square overturning lengths, were much smaller than Ozmidov scales, $L_{OZ} \equiv (\epsilon/N^3)^{1/2}$, indicating that the largest overturns were not limited by buoyancy.
 - (c) Surprisingly, temperature gradient spectra agreed with the Batchelor (1959) spectrum for scalar fluctuations in fully-developed turbulence. Consistent with the small overturning scales, magnitudes of the spectra were much smaller than typical and corresponded to a mixing efficiency, Γ , about 1% of typical values, e.g., $\Gamma \approx 0.0022$ versus $\Gamma = 0.24$ in a typical thermocline (Oakey 1982).
4. Three profiles in large aggregations, assumed to be fish, contributed half of the average turbulent dissipation in 142 profiles along a 5-km survey line during a 12.5-h tidal cycle. Although dissipation in the aggregations was 100 times background levels, the

accompanying diapycnal diffusivity, K_ρ , was about the same as outside the aggregations because the mixing efficiency was 100 times smaller.

Observed dissipation rates within the larger aggregations were surprisingly close in magnitude and internal uniformity to the ‘universal’ level of $\approx 10^{-5} \text{ W kg}^{-1}$ predicted by Huntley and Zhou (2004). Values at least 10 times smaller were observed in some aggregations, but lacking more information about their internal constituents and structure, it is not possible to know how much of the variability resulted from differences in composition and behavior of the nekton, e.g., which aggregations had uniform spacing and swimming behavior, and how much represented different stages of turbulent evolution or was simply statistical variability under-sampled by our few profiles. This applies even more strongly to estimates of mixing efficiency, as they are ratios of two microscale variances. Very low efficiency is consistent with Thorpe scales much smaller than Ozmidov scales, but efficiencies may vary more than shown by our estimates. We are at an early stage of understanding turbulence in fish schools.

Although environments, organisms, and swimming styles are quite different, rising krill in Saanich Inlet and nekton aggregations, probably anchovies, in Monterey Bay produced $\epsilon \approx 10^{-5}$. The data are too few and too little is known about the swimmers for general conclusions, but both observations are consistent with the conclusion by Huntley and Zhou (2004) that all swimming schools produce $\epsilon \approx 10^{-5} \text{ W kg}^{-1}$. Mixing efficiency is the major discrepancy. Kunze et al. (2006) state that the shear spectra they observed were consistent with the universal turbulent spectrum and that the Ozmidov scale represents the observed overturning scales. Finding non-universal shear spectra and overturning scales much smaller than the Ozmidov scale, we suggest that krill moving upward generate overturns more effectively

than did the mostly horizontal velocities in tail vortices of nekton swimming horizontally.

Velocity spectra peaking at 0.12 m (the inverse of 0.08 cpm) were roughly consistent with observed Thorpe scales of 0.04–0.2 m (Fig. 16) and with typical sizes of anchovies (≈ 0.12 m), the fish most likely to have formed these aggregations. Assuming horizontal isotropy, the observed root-mean-square (rms) velocity in one component of 4 mm s^{-1} probably represented a true velocity of 5.6 mm s^{-1} . For comparison, Huntley and Zhou (2004) use 140 mm s^{-1} for the northern anchovy, and a general rule-of-thumb is that cruising speeds are 1–2 body lengths per second (Weihs 1973), which translates to 120–240 mm s^{-1} for the 0.12-m body length we assumed for anchovy in Monterey Bay. We are not aware of a relationship between swimming speed and rms turbulent velocity and regard that as an issue for further investigation.

Turbulence produced by impulsive overturning of stratified profiles decays with a time scale of a buoyancy period (Itsweire et al. 1986), 5–15 min for the depths of the fish aggregations. Even for anchovies swimming at a minimal rate of one body length per second, i.e., 0.12 m s^{-1} , there would be little chance of turbulence decaying for a buoyancy period before another fish came by. Hence, it is likely that relatively uniform dissipation rates were observed because most of the turbulence was in a relatively early stage of decay.

Aligning MMP profiles with corresponding acoustic measurements maximizes the potential correlation between turbulence and fish dynamics. At a threshold of $-65 \text{ dB re } 1 \text{ m}^{-1}$, backscatter intensities in $1 - \text{m}^2$ cells of the MMP 15017 aggregation ranged from -65.0 to $-37.7 \text{ dB re } 1 \text{ m}^{-1}$. The corresponding MMP turbulent dissipation profile (15017) was highly correlated with volume backscatter measurements. In a contrasting example, acoustic backscatter values in the aggregation sampled by profile 15041 did not correlate with

dissipation rates, despite efforts to match spatial locations using offsets due to current flow measured using the ship’s ADCP. Correlations between the two measurement sets were also susceptible to movements of fish within aggregations. Observed high-intensity backscatter regions within aggregations suggest that packing densities may be spatially and temporally dynamic within fish aggregations (Rose 1993). Knowledge of diel and seasonal aggregation behavior associated with feeding and reproduction aids in acoustic species identification (Barange and Hampton 1997), and may explain variability observed in turbulence profiles. To illustrate by example, reported estimates of northern anchovy packing densities have ranged over three orders of magnitude from 0.5 to 533 fish m^{-3} (Graves 1974; Mais 1974; Hewitt 1975), depending on assumed fish length distributions and measurement techniques. Most of our estimates of packing density, i.e., N_f/V (Table 2), are in the range found for northern anchovies. Using $M = 0.013$ kg for anchovy, the packing density relation of Huntley and Zhou (2004) gives $N_f/V = 0.64 \text{ m}^{-1.2} = 0.0035 \text{ m}^{-3}$, slightly less than our smallest estimate. Ranges in packing densities of fish aggregations are not regularly reported.

Owing to the combination of intense dissipation rates and low mixing efficiency in aggregations, the diapycnal diffusivity, K_ρ , will be overestimated if dissipation contributions from aggregations are not recognized. Using the present data, the error would have been a factor of 2 for the outer part of Monterey Bay, not a huge discrepancy given current knowledge about mixing in the ocean. Nonetheless, acoustic backscatter should be monitored to obtain accurate diffusivities where aggregations occur. In our case, there were strong signatures in the 38-kHz ship’s echo sounder that would have identified the aggregations.

The prediction of greatly reduced mixing efficiency by Visser (2007) was prescient, although its rationale seems less so. Without comment or justification, Visser used the 4/3

law, proposed by Richardson (1926) for dispersion, not for diffusion, and obtained a functional dependence on ϵ and Γ to replace the universal constant assumed by Richardson. His assumptions require justification before the result,

$$\Gamma = \frac{L_{\text{TH}}^2}{L_{\text{OZ}}^2} \quad (7)$$

can be accepted as established. This expression, however, is proportional to the ratio of the turbulent potential energy, $\nabla PE = (1/2)N^2L_{\text{TH}}^2$, to the turbulent kinetic energy dissipated during a buoyancy period, $\nabla KE = 2\pi\epsilon/N$. Both have units of J kg^{-1} . Rearranging,

$$\frac{\nabla PE}{\nabla KE} = \frac{N^2L_{\text{TH}}^2/2}{2\pi\epsilon/N} = \frac{1}{4\pi} \frac{L_{\text{TH}}^2}{\epsilon/N^3} = \frac{1}{4\pi} \frac{L_{\text{TH}}^2}{L_{\text{OZ}}^2} \quad (8)$$

Only some of the turbulent potential energy will be converted to mean potential energy, as some displaced fluid will resettle near its initial position with little alteration. Therefore, this ratio is likely an upper bound for Γ rather than an accurate estimate.

A potential application of turbulence measurements within fish aggregations is to use dissipation rates to index behavior, packing densities, and possibly identify constituent species within aggregations. It is well documented that fish swimming styles differ among behaviors and species (Webb 1975; Videler and Nolet 1990). We do not know if turbulence measurements or changes in dissipation rates could be used to increase information and understanding of dynamics within fish and zooplankton aggregations.

Acknowledgments.

The Office of Naval Research funded this work as part of their program Assessing the Effects of Submesoscale Ocean Parameterizations (AESOP). JKH was supported through a

National Ocean Partnership Program (NOPP) grant funded by NOAA Ocean Exploration (NAO5OAR4601090). We are indebted to Jack Miller, Glenn Carter, Steve Bayer, Andrew Cookson, Keith Magness, Simon Kang, and Scott Lowiki for their dedicated efforts in collecting these data, and to Dave Winkel for his help with processing in addition to collection. Eric Buck (Captain) and the officers and crew of R/V *Revelle* also were essential in doing their utmost to comply with our sometimes unorthodox requests. Francisco Chavez and his colleagues at MBARI first suggested that the acoustic images indicated fish aggregations, most likely anchovies, and Brian Moore at BioSonics helped us understand system calibrations. David Barbee was very helpful in assisting with the analysis of the acoustic data. Steve Thorpe provided useful advice concerning mixing efficiency, and Eric Kunze contributed useful comments about the original manuscript.

APPENDIX

Observational Details

a. Modular Microstructure Profilers (MMPs)

Modular Microstructure Profilers (MMPs) 1 and 2 took all of the profiles analyzed here. Both carried two airfoils, a pumped Sea-Bird CTD, and an OBS-3 for particulates from D & A Instrument Co. The OBS-3 detects backscatter from an infrared beam centered on 875 nm that is down 3 dB at ± 35 nm. In pure water the beam has an e-folding distance of 50 mm. Initially, the MMPs had Fastip thermistors for χ_T as well as for well-resolved temperature profiles. Halfway through the cruise, the FP07s were replaced with Sea-Bird dissolved oxygen probes used to track water masses (MMPs do not have enough data channels to record oxygen and temperature microstructure simultaneously.) All Sea-Bird probes were calibrated before and after the cruise. Comparison of temperature spectra of Sea-Bird temperature and FP07 thermistors demonstrates that the Sea-Bird probes are increasingly attenuated at high frequencies as length scales become smaller than 1 m. The airfoils were calibrated in a water jet at APL-UW, and the low-frequency portions of FP07 records were calibrated in situ by comparison with the more stable Sea-Bird temperature probes. Fall rates were 0.6–0.7 m s⁻¹, and a small acoustic altimeter measured height above the bottom. Although Sea-Bird temperature and conductivity are pumped, the data must be filtered and offset to minimize salinity spiking, which progressively attenuates signals smaller than 1 m.

We computed airfoil spectra over sequential half-overlapping intervals 1.5 m long using four multitapers with Riedel weights (Percival and Walden 1993) After applying transfer functions for electronic and probe characteristics to produce shear spectra (Moum et al. 1995), we integrated the spectra to obtain $\overline{(\partial u / \partial z)^2}$. Assuming full isotropy,

$$\epsilon = 7.5\nu\overline{(\partial u / \partial z)^2} \quad [\text{W kg}^{-1}] \quad (\text{A1})$$

b. Echosounder data collection

Acoustic reflectivity, i.e., backscatter, was measured using a BioSonics DTX echosounder operating at 120 and 208 kHz. The transducers were mounted in the instrument well located in the R/V *Revelle* hangar, 4 m below the ship's water line.

The acoustic data are analyzed and displayed in terms of the volume backscattering strength, S_v , which Urick (1975) defines as

$$S_v \equiv 10 \log_{10} \frac{p_{\text{scattered}}^2}{p_{\text{incident}}^2} \quad [\text{dB re } 1 \text{ m}^{-1}] \quad (\text{A2})$$

In terms of the sonar equation,

$$S_v = RL - SL + TL - 10 \log_{10} V \quad (\text{A3})$$

where $RL \equiv 10 \log_{10} p^2$ is the received pressure in units of dB relative to $1\mu\text{Pa}$ at the receiver; SL is the source level, $TL = 40 \log_{10} r + 2\alpha(S, T, p)r$ is the two-way transmission loss, where r is the range in meters and $\alpha(S, T, p)$ is the absorption coefficient. Using tables in Garrison (1994) and water properties observed with the Sea-Bird CTDs on the MMPs, the data were analyzed using $\alpha = 0.0395$ at 120 kHz and 0.0568 at 208 kHz. Source levels were 223.0

and 224.5 dB re 1 m⁻¹ from the transducers, and the receiver sensitivities were -47.2 and -48.0 dB re 1 m⁻¹. The acquisition threshold was set at -130 dB re 1 m⁻¹.

V is the scattering volume. Following Urick (1975) and BioSonics (2004), it is determined using

$$-10 \log_{10} V = -10 \log_{10} \left(\frac{c \tau_{pulse}}{2} \right) - 20 \log_{10} r - 10 \log_{10} \Psi \quad (\text{A4})$$

where c is the sound speed, $\tau_{pulse} = 400 \mu\text{s}$ is the duration of the transmitted pulse, and Ψ is the half-power beam width, i.e., 3 dB below peak intensity, which is 7° and 6.2° at 120 and 208 kHz, respectively.

Pelagic patches of intense backscatter coincident with turbulence profiles were identified and characterized using Echoview (version 4.2) software. Patch boundaries were delineated using the SHAPES algorithm (Coetzee 2000) implemented in Echoview. Aggregations were detected and characterized at a -65 dB re 1 m⁻¹ backscatter threshold (ICES 2000). Values for the six additional input parameters: minimum candidate length (MCL), minimum candidate height (MCH), minimum school length (MSL), minimum school height (MSH), maximum vertical linking distance (MVLD), and maximum horizontal linking distance (MHLD) needed for the school detection algorithm are listed in Table 2.

c. Batchelor spectrum for thermal microstructure

Grant et al. (1968) express the one-dimensional form of the Batchelor spectrum for the

viscous-diffusive subrange temperature fluctuations in water as

$$\begin{aligned}\Phi_T^{\text{Batchelor}}(k_1) &= 2\sqrt{\pi}q^{3/2}\kappa_T^{1/2}\nu^{3/4}\epsilon^{-3/4}\chi_T \left(\frac{e^{-a^2/2}}{a\sqrt{2\pi}} - \int_a^\infty \frac{e^{-y^2/2}}{\sqrt{2\pi}} dy \right) \quad [\text{K}^2\text{cpm}^{-1}] \\ &= 2\sqrt{\pi}q^{3/2}\kappa_T^{1/2}\nu^{3/4}\epsilon^{-3/4}\chi_T \left(\frac{e^{-a^2/2}}{a\sqrt{2\pi}} - \frac{\text{erfc}(a/\sqrt{2})}{2} \right)\end{aligned}\quad (\text{A5})$$

where $a \equiv \sqrt{2q}k_1/k_B$, and, as used in Matlab R2007b, the complimentary error function is $\text{erfc}(x) = (2/\sqrt{\pi}) \int_x^\infty e^{-t^2} dt$, and k_1 is a one-dimensional wavenumber in cycles per meter (cpm). The parameters are the molecular diffusivity, κ_T , the kinematic viscosity, ν , the rate of viscous dissipation of turbulent kinetic energy, ϵ , and the rate of diffusive dissipation of turbulent temperature fluctuations, χ_T . Batchelor (1959) estimates the least principal rate of strain in fully-developed turbulence as $-\sqrt{\epsilon/\nu}/q$. By comparing velocity and temperature microstructure in the ocean, Oakey (1982) estimated $q = 3.7 \pm 1.5$. Units of (A5) are $\text{K}^2/(\text{radian}/\text{m})$, where K represents degrees Kelvin. Here, (A5) was multiplied by 2π to convert spectral units to K^2/cpm .

The gradient form of the Batchelor spectrum was computed as

$$\Phi_{TG}^{\text{Batchelor}}(k_1) = (2\pi k_1)^2 \Phi_T^{\text{Batchelor}}(k_1) \quad [(\text{K}/\text{m})^2\text{cpm}^{-1}] \quad (\text{A6})$$

REFERENCES

- Barange, M. and I. Hampton, 1997: Spatial structure of co-occurring anchovy and sardine populations from acoustic data: implications for survey design. *Fish. Oceanogr.*, **6**, 94–108.
- Barange, M., I. Hampton, and M. Soule, 1996: Empirical determination of the in-situ target strengths of three loosely aggregated pelagic fish species. *ICES J. Mar. Sci.*, **53**, 225–232.
- Batchelor, G. K., 1959: Small-scale variation of convected quantities like temperature in turbulent fluid. *J. Fluid Mech.*, **5**, 113–139.
- BioSonics, 2004: DT4 data file format specification. Tech. rep., BioSonics Inc., 31 pp., 4027 Leary Way NW, Seattle, WA 98107.
- Boden, B., M. Johnson, and E. Brinton, 1955: The euphausiidae (crustacea) of the North Pacific. *Bull. Scripps Inst. Oceanogr.*, **6**, 287–400.
- Cheng, J.-Y. and G. Chahine, 2001: Computational hydrodynamics of animal swimming: boundary element method and three-dimensional vortex wake structure. *Comp. Biochem. and Physiol., A*, **131**, 51–60.
- Coetzee, J., 2000: Use of a shoal analysis and patch estimation system (shapes) to characterize sardine schools. *Aquat. Liv. Res.*, **13**, 1–10.
- Conti, S. and D. Demer, 2003: Wide-bandwidth acoustical characterization of anchovy and

- sardine from reverberation measurements in an echoic tank. *ICES J. Mar. Sci.*, **60**, 617–624.
- Croll, D., B. Marinovic, B. Benson, F. Chavez, N. Black, N. Black, R. Ternullo, and B. Tershy, 2005: From wind to whales: trophic links in a coastal upwelling system. *Mar. Ecol. Prog. Ser.*, **289**, 117–130.
- Dewar, W., R. Bingham, R. Iverson, D. Nowacek, L. S. Laurent, and P. Wiebe, 2006: Does the marine biosphere mix the ocean? *J. Mar. Res.*, **64**, 541–561.
- Dillon, T. M., 1982: Vertical overturns: A comparison of Thorpe and Ozmidov length scales. *J. Geophys. Res.*, **87**, 9601–9613.
- Farmer, D., G. Crawford, and T. Osborn, 1987: Temperature and velocity microstructure caused by swimming fish. *Limnol. Oceanogr.*, **32** (4), 978–983.
- Fiedler, P., et al., 1998: Blue whale habitat and prey in the California Channel Islands. *Deep-Sea Res. II*, **45**, 1781–1801.
- Foote, K., 1983: Linearity of fisheries acoustics, with addition theorems. *J. Acoust. Soc. Am.*, **73**, 1932–1940.
- Gargett, A. E., T. R. Osborn, and P. W. Nasmyth, 1984: Local isotropy and the decay of turbulence in a stratified fluid. *J. Fluid Mech.*, **144**, 231–280.
- Garrett, C. J. R. and W. H. Munk, 1975: Space-time scales of internal waves: A progress report. *J. Geophys. Res.*, **80**, 291–297.

- Garrison, 1994: APL-UW high-frequency ocean environmental acoustic models handbook. Tech. Rep. APL-UW TR 9407, Applied Physics Laboratory, University of Washington, 216 pp., 1013 NE 40th St., Seattle, WA 98105-6698.
- Grant, H., B. Hughes, W. Vogel, and A. Moilliet, 1968: The spectrum of temperature fluctuations in turbulent flow. *J. Fluid Mech.*, **34**, 423–442.
- Graves, J., 1974: Three dimensional spacing in pelagic fish schools determined by photography. Tech. Rep. LJ-74-44, Nat. Mar. Fish. Serv., SW Fish Center, 1–9 pp., La Jolla, CA 92037.
- Gregg, M., E. D’Asaro, T. Shay, and N. Larson, 1986: Observations of persistent mixing and near-inertial internal waves. *J. Phys. Oceanogr.*, **16**, 856–885.
- Gregg, M. C., D. P. Winkel, T. B. Sanford, and H. Peters, 1996: Turbulence produced by internal waves in the oceanic thermocline at mid and low latitudes. *Dyn. Atmos. Oceans*, **24**, 1–14.
- Hewitt, R., 1975: Sonar mapping in the California Current area: A review of recent developments. Tech. Rep. 18, Calif. Coop. Oceanic Fish Investigation, 149–154 pp.
- Hewitt, R., P. Smith, and J. Brown, 1976: Development and use of sonar mapping for pelagic stock assessment in the California current area. *U.S. Fish. Bull.*, **74**, 281–300.
- Huntley, M. and M. Zhou, 2004: Influence of animals on turbulence in the sea. *Mar. Ecol. Prog. Ser.*, **273**, 65–79.

- ICES, 2000: Report on echo trace classification. *ICES Coop. Res. Rept. 238*, R. Reid, Ed., Intl. Council Explor. Sea, Copenhagen, Denmark, 107.
- Itsweire, E. C., K. N. Helland, and C. W. Van Atta, 1986: The evolution of grid-generated turbulence in a stratified fluid. *J. Fluid Mech.*, **162**, 299–338.
- Kunze, E. and J. Dower, 2007: Response to tom p. rippeth et al. *Science Online*.
- Kunze, E., J. Dower, I. Beveridge, R. Dewey, and K. Bartlett, 2006: Observations of biologically generated mixing in a coastal inlet. *Science*, **313**, 1768–1770.
- Mais, K., 1974: Pelagic fish surveys in the California Current. *U.S. Fish Bull.*, **18**, 149–154.
- Moum, J., 1996: Efficiency of mixing in the main thermocline. *J. Geophys. Res.*, **101**, 12,057–12,069.
- Moum, J. N., M. C. Gregg, R. C. Lien, and M. E. Carr, 1995: Comparison of turbulent kinetic energy dissipation rate estimates from two ocean microstructure profilers. *J. Atmos. Ocean. Tech.*, **12**, 346–366.
- Muller, U., B. V. D. Heuvel, E. Stamhuis, and J. Videler, 1997: Fish foot prints: morphology and energetics of the wake behind a continuously swimming mullet (*chelon labrosus risso*). *J. Exp. Biol.*, **200**, 2893–2906.
- Munk, W., 1966: Abyssal recipes. *Deep-Sea Res.*, **13**, 707–730.
- Oakey, N. S., 1982: Determination of the rate of dissipation of turbulent energy from simultaneous temperature and velocity shear microstructure measurements. *J. Phys. Oceanogr.*, **12**, 256–271.

- Osborn, T. R., 1980: Estimates of the local rate of vertical diffusion from dissipation measurements. *J. Phys. Oceanogr.*, **10**, 83–89.
- Osborn, T. R. and C. S. Cox, 1972: Oceanic fine structure. *Geophys. Fluid Dyn.*, **3**, 321–345.
- Panchev, S. and D. Kesich, 1969: Energy spectrum of isotropic turbulence at large wavenumbers. *Comptes rendus de l'Académie bulgare des Sciences*, **22**, 627–630.
- Percival, D. and A. Walden, 1993: *Spectral Analysis for Physical Applications*. Cambridge Univ. Press, Cambridge, U.K., 583 pp.
- Peters, H., M. Gregg, and J. Toole, 1988: On the parameterization of equatorial turbulence. *J. Geophys. Res.*, **93**, 1199–1218.
- Richardson, L., 1926: Atmospheric diffusion shown on a distance-neighbor graph. *Proc. Roy. Soc. London, A*, **97**, 354–373.
- Rippeth, T., J. Gascoigne, , J. Greene, M. Inall, M. Palmer, J. Simpson, and P. Wiles, 2007: Turbulent dissipation in coastal seas. *Science Online*.
- Rose, G., 1993: Cod spawning on a migration highway in the north-west Atlantic. *Nature*, **366**, 458–461.
- Schoenherr, J., 1991: Blue whales feeding on high concentrations of euphausiids around Monterey submarine canyon. *Can. J. Zool.*, **69**, 583–594.
- Smith, P., 1970: The horizontal dimensions and abundance of fish schools in the upper mixed layer as measured by sonar. *Proceedings of an International Symposium on Biolog-*

- ical Sound Scattering in the Ocean*, G. Farquhar, Ed., Maury Center for Ocean Science, Washington, D.C., 563–600.
- Thorpe, S. A., 1977: Turbulence and mixing in a Scottish Loch. *Phil. Trans. Roy. Soc. London*, **286**, 125–181.
- Urick, R., 1975: *Principles of Underwater Sound*. McGraw-Hill, New York, 384 pp.
- Videler, J. and B. Nolet, 1990: Costs of swimming measured at optimum speed: scale effects, differences between swimming styles, taxonomic groups and submerged and surface swimming. *Comp. Biochem. Physiol. A*, **97**, 91–99.
- Videler, J., E. Stamhuis, U. Muller, and L. van Duren, 2002: The scaling and structure of aquatic animal wakes. *Integr. Comp. Biol.*, **42**, 988–996.
- Visser, A., 2007: Biomixing of the oceans? *Science*, **316**, 838–839.
- Webb, P., 1975: Hydrodynamics and energetics of fish propulsion. *Bull. Fish. Res. Board Can.*, **190**, 1–159.
- Weihs, D., 1973: Optimal fish cruising speed. *Nature*, **245**, 48–50.

List of Figures

- 1 Logarithm of the turbulent dissipation rate (upper panel) and east/west velocity observed with the R/V *Revelle* hydrographic ship sonar (lower panel) during MMP Group 2, Sub 6. Top axis, upper panel is time in decimal year day, and the red crosses are times profiles began. Bottom axis, distance along the track from the first profile. The color bar below the lower panel is velocity in m s^{-1} , and the bottom axis is year day. 40

- 2 Volume backscattering strength, S_v , in dB re 1 m^{-1} , at 120 kHz in grayscale overlaid with $\log_{10}(\epsilon/W \text{ kg}^{-1})$ in color from MMP profiles. Distances are relative to fixed waypoints for MMP groups, and the profiles are sequential designators of MMP profiles. Data shown are from: A) Group 2, Sub 6, starting at $121^{\circ} 53.77' \text{ W}$, $36^{\circ} 42.44' \text{ N}$, 1153 local time on 13 August and lasting 14.4 min; B) Group 2, Sub 7, starting at $121^{\circ} 53.68' \text{ W}$, $36^{\circ} 42.84' \text{ N}$, 1409 local on 13 August and lasting 7.2 min; C) Group 2, Sub 8, starting at $121^{\circ} 54.41' \text{ W}$, $36^{\circ} 41.21' \text{ N}$, 1531 local on 13 August and lasting 6.5 min; D) Group 14, Sub 1, starting at $121^{\circ} 54.24' \text{ W}$, $36^{\circ} 42.02' \text{ N}$, 0345 local on 22 August and lasting 20.2 min. 41

- 3 Summary of MMP 15018, taken during Group 2, Sub 6 and immediately after the profile that sampled the large aggregation in Figure 2A. Left) Potential temperature, salinity, potential density, and intensity of optical backscatter, which is proportional to the density of suspended particles. Middle Left) ϵ and the volume backscatter strength, S_v , interpolated from the depth-distance MMP trajectory. Middle Right) Buoyancy Reynolds number, $Re_B \equiv \epsilon/\nu N^2$. Right) Stratification, N^2 , and shear² over 4-m intervals. Outside the aggregation in Figure 2A, moderately strong turbulence occurred in the layer centered near 0.3 MPa, and intense turbulence was centered on the homogeneous layer at 0.6 MPa. Elsewhere, Re_B was generally too small to justify assuming isotropy. 42
- 4 Summary of MMP 15017 through the large, intense fish aggregation in Figure 2B. In the same format as the previous figure, this profile is distinguished from nearby ones outside aggregations only by ϵ and Re_B . There is no significant difference in the stratification. 43
- 5 Summary of MMP 15041 (MMP Group 2, Sub 7, 1409 local on 13 August). Unlike the previous examples, here S_v shows little correlation with ϵ , which rises to levels found in the previous aggregations only between 0.5 and 0.7 MPa. This, and other evidence presented in the text, indicates that the computed depth-distance MMP trajectory was off, resulting in an erroneous interpolation of S_v . It is likely that the profiler penetrated the aggregation only between 0.5 and 0.7 Pa. 44

6	<p>Summary of MMP 15057 in a small aggregation that the profiler seems to have entered sooner than indicated by S_v interpolated onto the calculated trajectory. Both the magnitude and uniformity of ϵ indicate that the profiler was inside the aggregation, or water very recently disturbed by the fish, from about 0.3 MPa to just above the bottom at 0.81 MPa.</p>	45
7	<p>Summary of MMP 17259, taken through the third and largest of the three aggregations in Figure 2D. It was near the locations of 15017 and 15041 but nine days later. S_v and $\log_{10}(\epsilon)$ are about 10 dB smaller than MMP 15017 (Fig. 4) but are as highly correlated.</p>	46
8	<p>Upper) Average shear spectrum over 0.3–0.6 MPa in MMP 15017, spanning the large fish aggregation sampled by that profile. Thin lines are upper and lower 95% confidence limits, and the dotted spectrum is the Panchev and Kesich (1969) universal shear spectrum for $\epsilon = 2.78 \times 10^{-6} \text{ W kg}^{-1}$. Lower) Variance-preserving forms of the same spectra reveal that the low-wavenumber departure from the universal form has a negligible effect on shear variance. Multitaper spectra were taken in sequential blocks of 1000 samples using Riedel weights with four tapers. Instrument vibrations dominate the spectrum for $k > 100 \text{ cpm}$.</p>	47

9	Average shear spectrum over 0.50–0.65 MPa in MMP 15018, the most turbulent section of a typical profile on the Monterey shelf and not in an aggregation. This section has an average dissipation rate of $\epsilon = 4.92 \times 10^{-8} \text{ W kg}^{-1}$ and is centered on a well-mixed layer (Fig. 3). Although $\bar{\epsilon}$ is only 1/50th of that in the aggregation sampled by MMP 15017, the spectrum is close to the universal form at all wavenumbers.	48
10	Velocity spectrum in the fish aggregation sampled by MMP 15017. The spectrum and its variance-preserving form correspond to the shear spectra in Fig. 8. Owing to the low-wavenumber falloff, the variance-preserving form peaks at 8 cpm.	49
11	Average velocity spectrum not in a fish aggregation, corresponding to the MMP 15018 shear spectra in Fig. 9. The spectrum and its variance-preserving form are close to the universal form without peaking at these wavenumbers.	50
12	Left) MMP 15017 FP07 temperature where the mean gradient is nearly linear within the large fish aggregation. Right) The observed temperature gradient spectrum overlaid with a theoretical spectrum consisting of the advective subrange, having a slope of $k^{1/3}$ below 4 cpm, and at higher wavenumbers the Batchelor spectrum for $\epsilon = 2.34 \times 10^{-6} \text{ W kg}^{-1}$. Fitting the Batchelor spectrum to the observed spectrum gave $C = 850$, or $K_T = 1.21 \times 10^{-4} \text{ m}^2 \text{ s}^{-1}$ and $\Gamma = 0.0026$	51

- 13 Left) MMP 15018 FP07 temperature where the mean gradient is nearly linear and not in a fish aggregation. Right) The observed temperature gradient spectrum overlaid with the Batchelor spectrum evaluated with $\epsilon = 2.62 \times 10^{-8} \text{ W kg}^{-1}$. Its fit to the observed spectrum gave $C = 250$, or $K_T = 3.57 \times 10^{-5} \text{ m}^2 \text{ s}^{-1}$ and $\Gamma = 0.203$ 52
- 14 TS relations of MMP 15017 (thick) and of three nearby profiles (thin). Depth increments of 10 m are marked with circles, some of which are labeled. Linearity between about 30 and 65 m permits estimating overturning scales from temperature. 53
- 15 Left) representative Ozmidov and Thorpe scales outside (MMP 15016) and inside (MMP 15017) aggregations, Middle) bandpassed raw airfoil signals, and Right) raw FPO7 temperature gradient signals. Note that the velocity scale for MMP 15017 is 10 times that of MMP15016, and its overturning scale is four times larger. MMP 15017 started in a low-density shallow extension above the main aggregation, which was between 0.3 and 0.6 MPa. Ozmidov scales greatly exceed Thorpe scales throughout, unlike the situation in MMP 15016, where the good agreement is typical of that found by many investigators. 54
- 16 Scatter plot of Thorpe scales, i.e., observed root-mean-square overturning scales, versus Ozmidov scales, L_{OZ} , for MMP profiles 15015–15018. Within aggregations Thorpe scales are likely to be much smaller than Ozmidov scales. 55

17 Left) Averages of a) the 142 dissipation profiles comprising Group 2, b) the three profiles in large, intense fish aggregations, and c) the 139 profiles not in large aggregations. Right) Average K_ρ of the 139 profiles not in large aggregations using $\Gamma = 0.2$ and for the three profiles in aggregations using $\Gamma = 0.0022$, the average efficiency found in aggregations. Although ϵ in aggregations averages 100 times that outside, the lower efficiency compensates, resulting in no significant difference in K_ρ inside and outside of the aggregations. 56

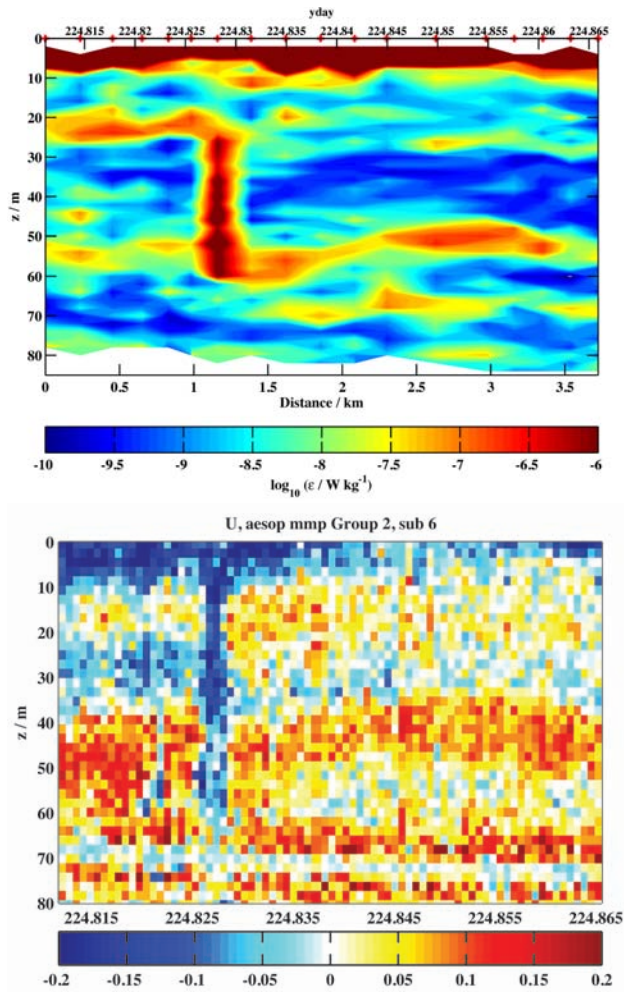


FIG. 1. Logarithm of the turbulent dissipation rate (upper panel) and east/west velocity observed with the R/V *Revelle* hydrographic ship sonar (lower panel) during MMP Group 2, Sub 6. Top axis, upper panel is time in decimal year day, and the red crosses are times profiles began. Bottom axis, distance along the track from the first profile. The color bar below the lower panel is velocity in m s^{-1} , and the bottom axis is year day.

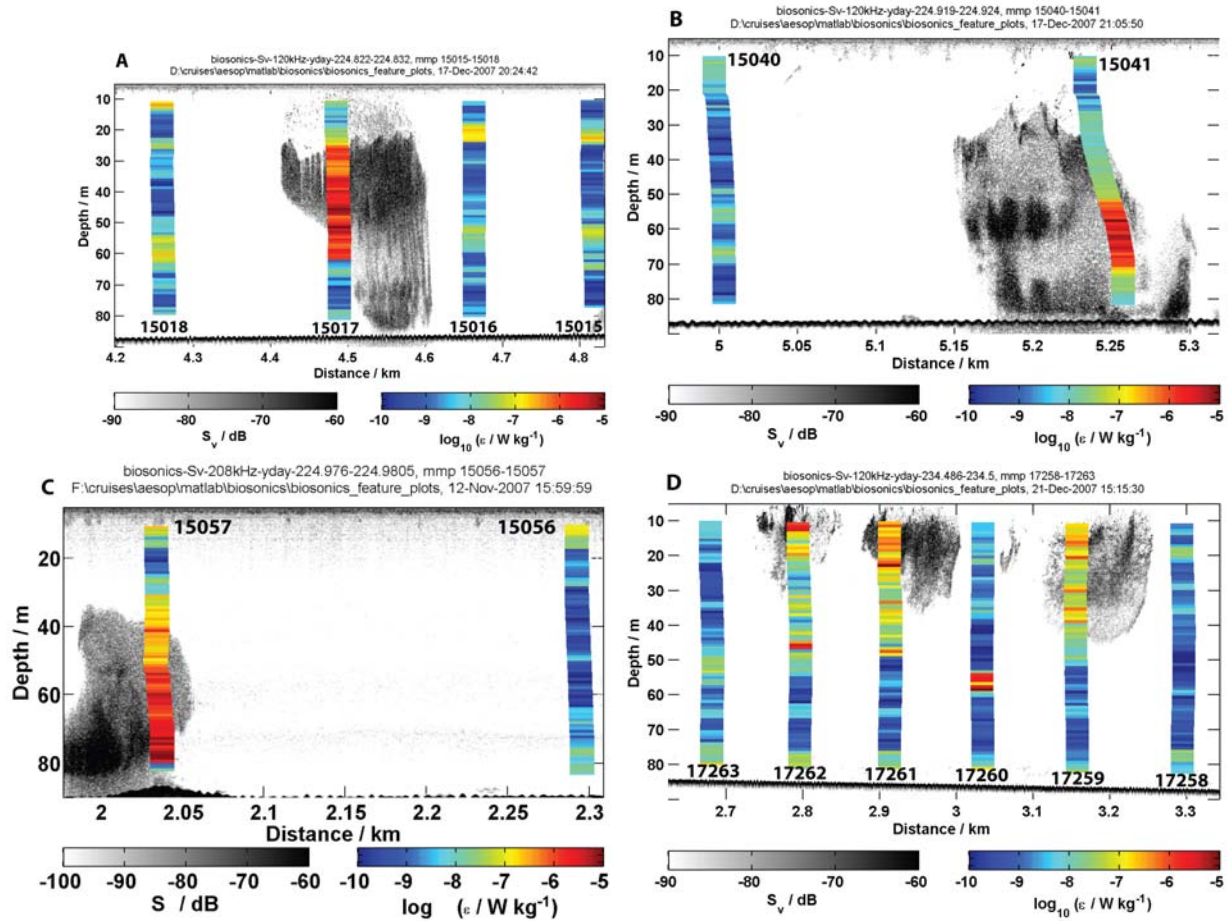


FIG. 2. Volume backscattering strength, S_v , in dB re 1 m^{-1} , at 120 kHz in grayscale overlaid with $\log_{10}(\epsilon/W \text{ kg}^{-1})$ in color from MMP profiles. Distances are relative to fixed waypoints for MMP groups, and the profiles are sequential designators of MMP profiles. Data shown are from: A) Group 2, Sub 6, starting at $121^{\circ} 53.77' \text{ W}$, $36^{\circ} 42.44' \text{ N}$, 1153 local time on 13 August and lasting 14.4 min; B) Group 2, Sub 7, starting at $121^{\circ} 53.68' \text{ W}$, $36^{\circ} 42.84' \text{ N}$, 1409 local on 13 August and lasting 7.2 min; C) Group 2, Sub 8, starting at $121^{\circ} 54.41' \text{ W}$, $36^{\circ} 41.21' \text{ N}$, 1531 local on 13 August and lasting 6.5 min; D) Group 14, Sub 1, starting at $121^{\circ} 54.24' \text{ W}$, $36^{\circ} 42.02' \text{ N}$, 0345 local on 22 August and lasting 20.2 min.

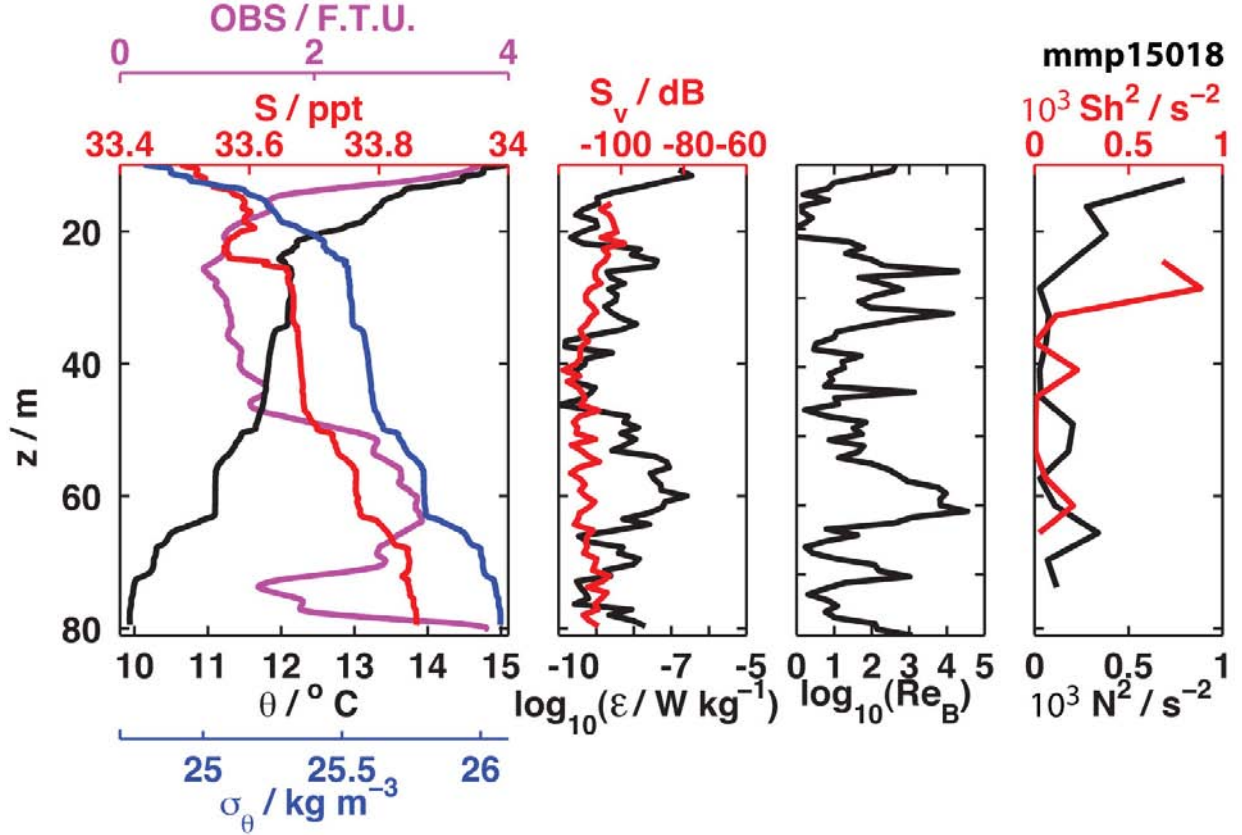


FIG. 3. Summary of MMP 15018, taken during Group 2, Sub 6 and immediately after the profile that sampled the large aggregation in Figure 2A. Left) Potential temperature, salinity, potential density, and intensity of optical backscatter, which is proportional to the density of suspended particles. Middle Left) ϵ and the volume backscatter strength, S_v , interpolated from the depth-distance MMP trajectory. Middle Right) Buoyancy Reynolds number, $Re_B \equiv \epsilon/\nu N^2$. Right) Stratification, N^2 , and shear² over 4-m intervals. Outside the aggregation in Figure 2A, moderately strong turbulence occurred in the layer centered near 0.3 MPa, and intense turbulence was centered on the homogeneous layer at 0.6 MPa. Elsewhere, Re_B was generally too small to justify assuming isotropy.

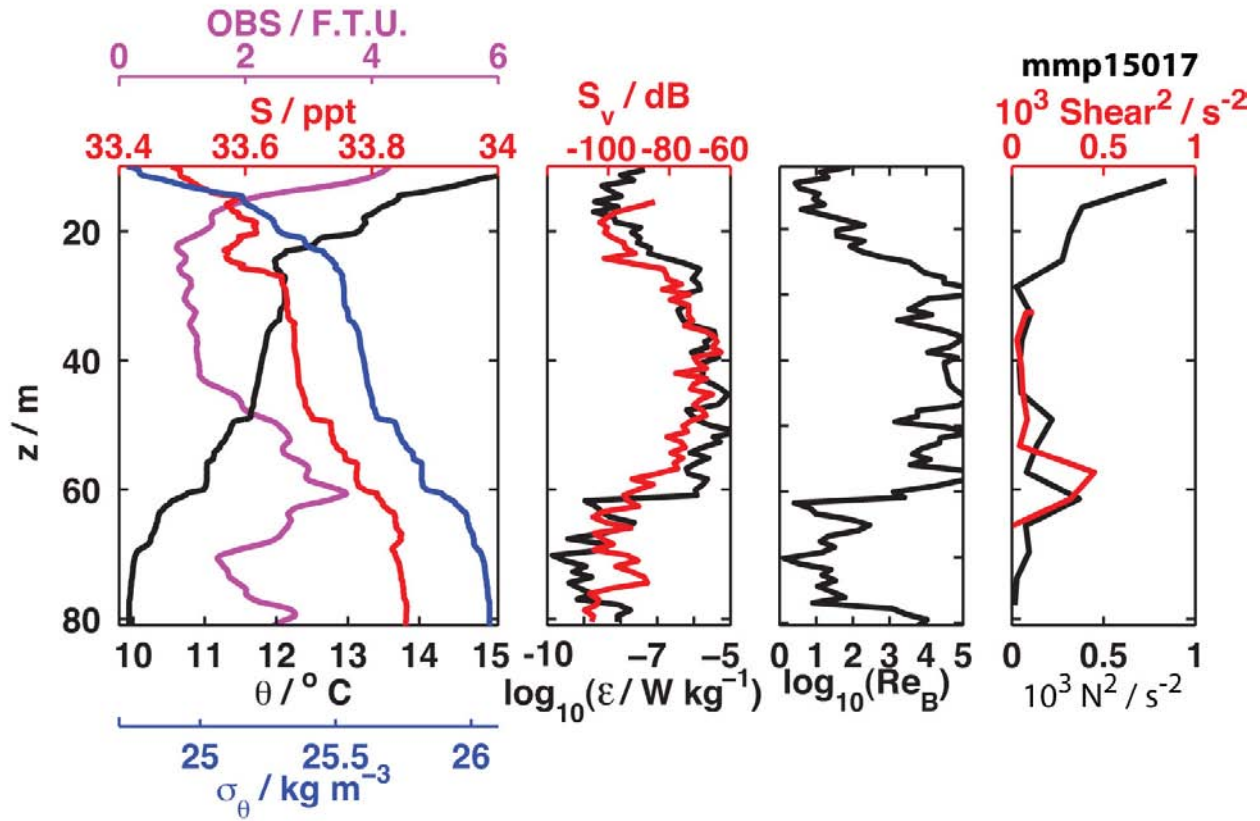


FIG. 4. Summary of MMP 15017 through the large, intense fish aggregation in Figure 2B. In the same format as the previous figure, this profile is distinguished from nearby ones outside aggregations only by ϵ and Re_B . There is no significant difference in the stratification.

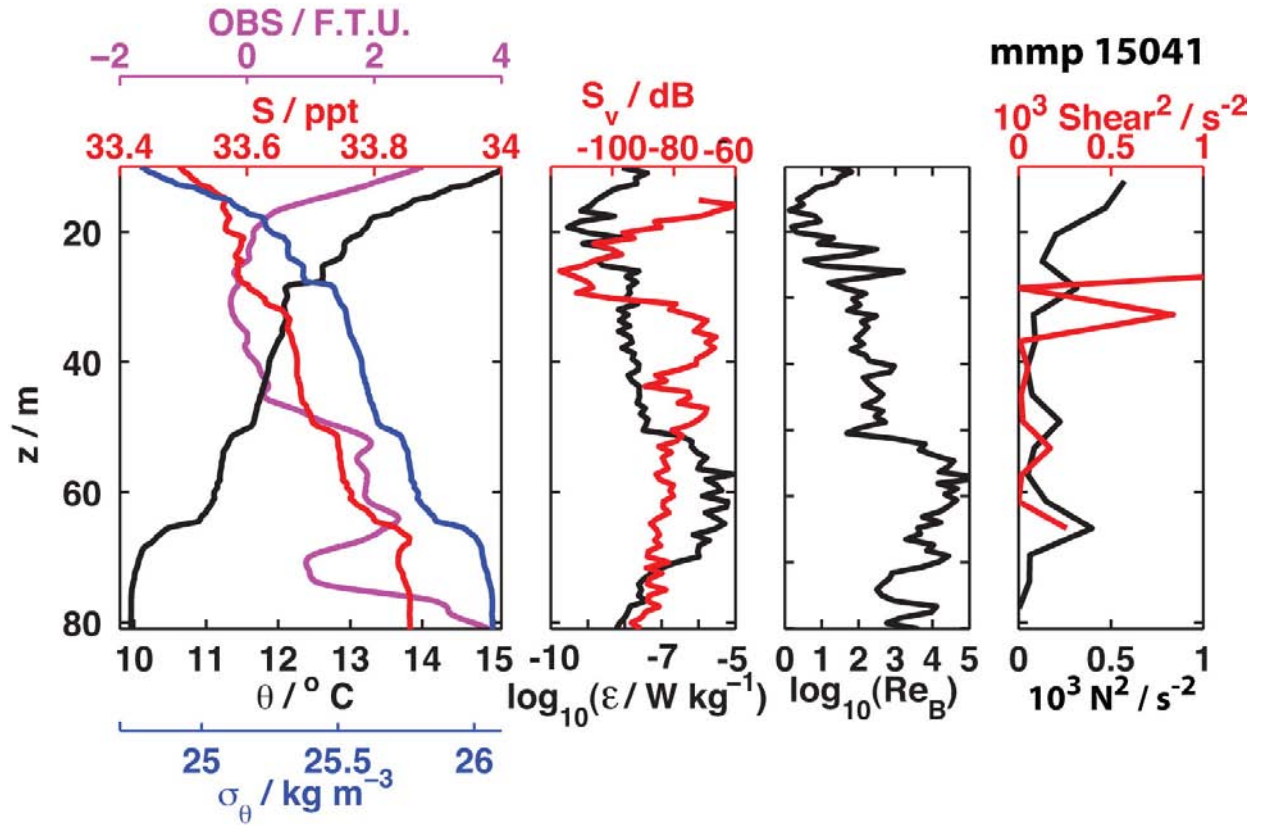


FIG. 5. Summary of MMP 15041 (MMP Group 2, Sub 7, 1409 local on 13 August). Unlike the previous examples, here S_v shows little correlation with ϵ , which rises to levels found in the previous aggregations only between 0.5 and 0.7 MPa. This, and other evidence presented in the text, indicates that the computed depth-distance MMP trajectory was off, resulting in an erroneous interpolation of S_v . It is likely that the profiler penetrated the aggregation only between 0.5 and 0.7 Pa.

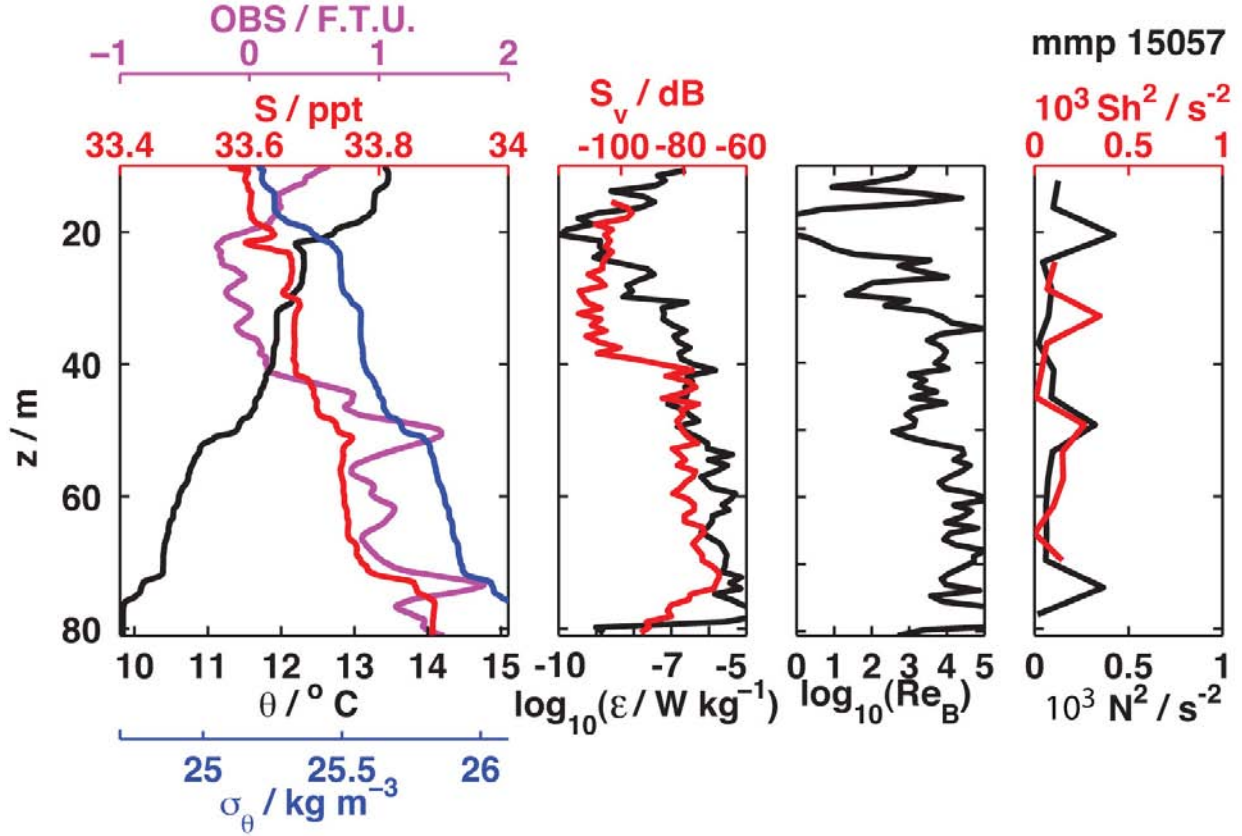


FIG. 6. Summary of MMP 15057 in a small aggregation that the profiler seems to have entered sooner than indicated by S_v interpolated onto the calculated trajectory. Both the magnitude and uniformity of ϵ indicate that the profiler was inside the aggregation, or water very recently disturbed by the fish, from about 0.3 MPa to just above the bottom at 0.81 MPa.

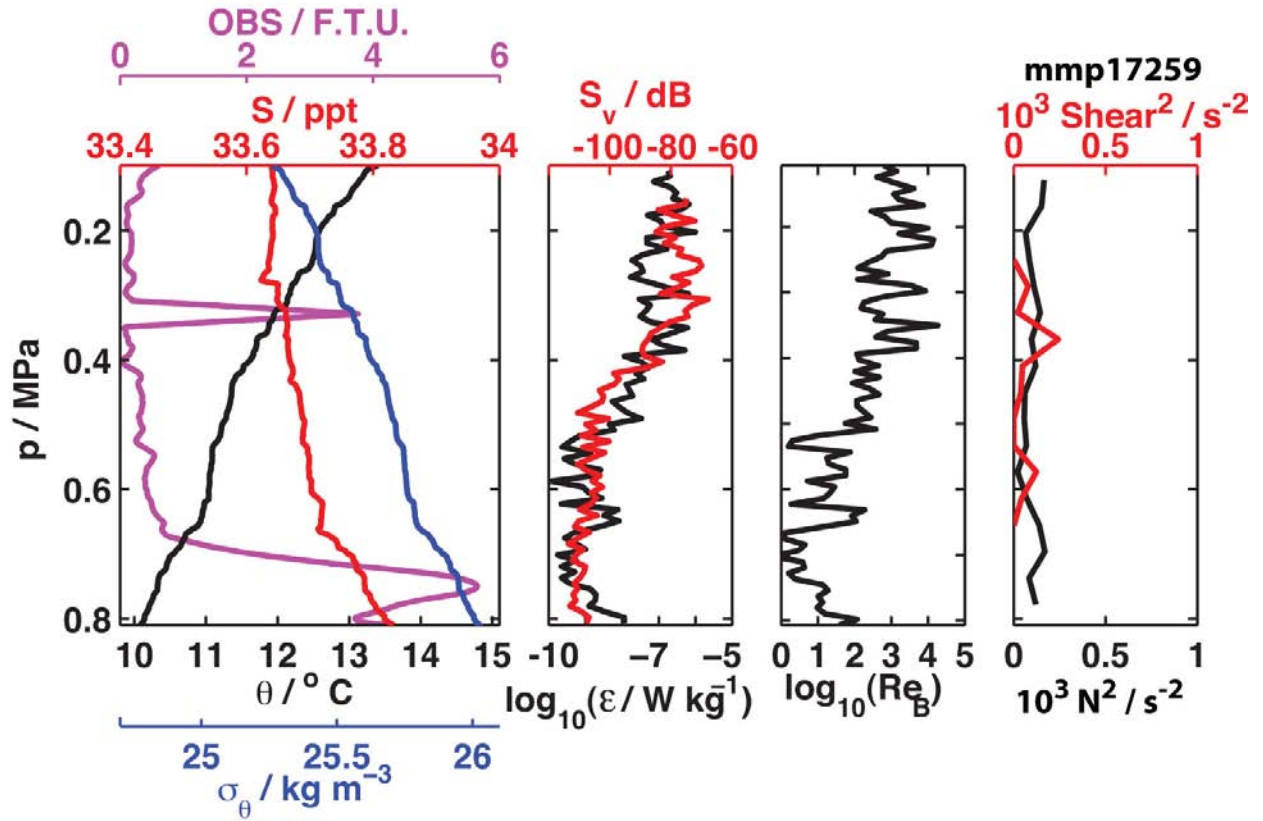


FIG. 7. Summary of MMP 17259, taken through the third and largest of the three aggregations in Figure 2D. It was near the locations of 15017 and 15041 but nine days later. S_v and $\log_{10}(\epsilon)$ are about 10 dB smaller than MMP 15017 (Fig. 4) but are as highly correlated.

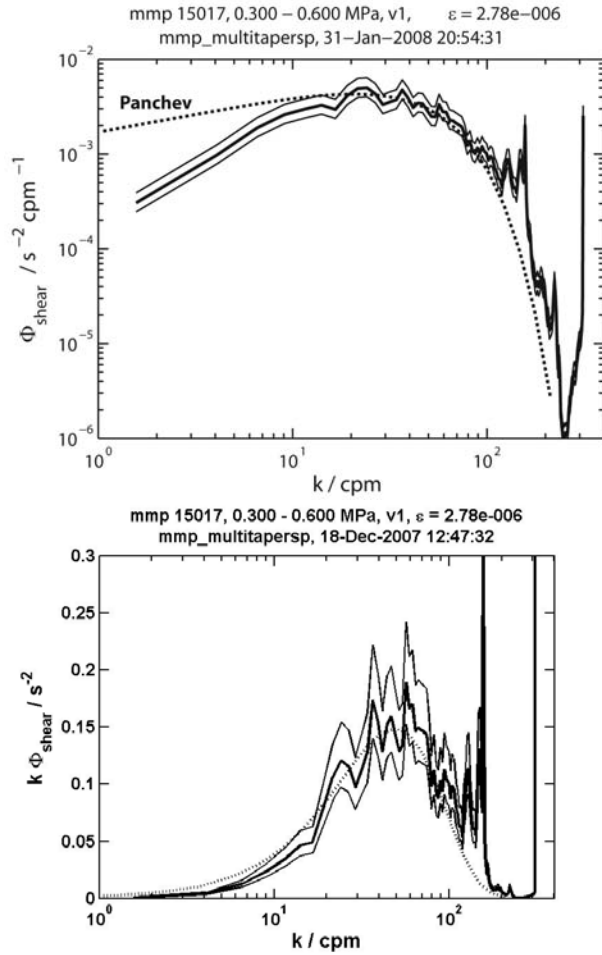


FIG. 8. Upper) Average shear spectrum over 0.3–0.6 MPa in MMP 15017, spanning the large fish aggregation sampled by that profile. Thin lines are upper and lower 95% confidence limits, and the dotted spectrum is the Panchev and Kesich (1969) universal shear spectrum for $\epsilon = 2.78 \times 10^{-6} \text{ W kg}^{-1}$. Lower) Variance-preserving forms of the same spectra reveal that the low-wavenumber departure from the universal form has a negligible effect on shear variance. Multitaper spectra were taken in sequential blocks of 1000 samples using Riedel weights with four tapers. Instrument vibrations dominate the spectrum for $k > 100$ cpm.

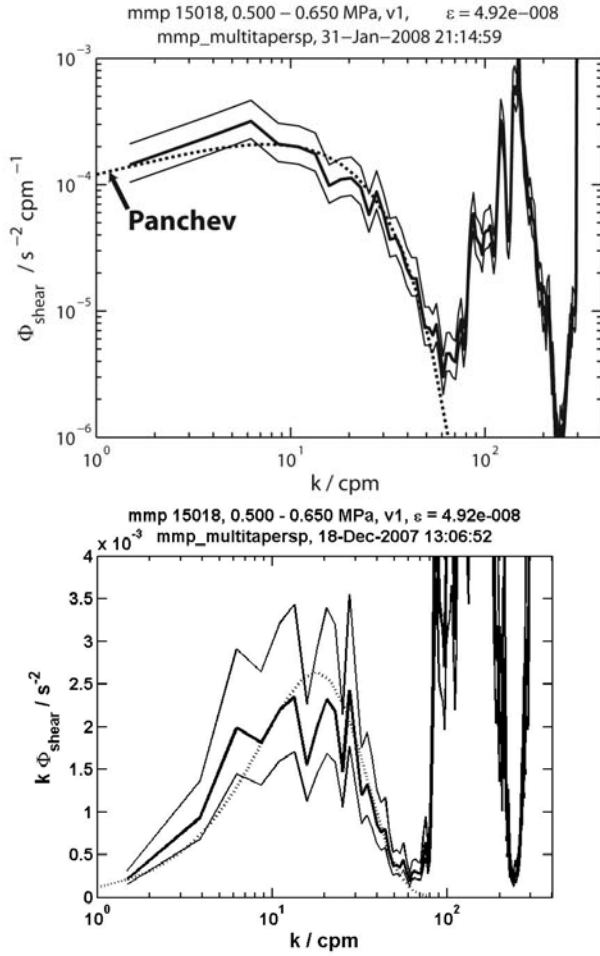


FIG. 9. Average shear spectrum over 0.50–0.65 MPa in MMP 15018, the most turbulent section of a typical profile on the Monterey shelf and not in an aggregation. This section has an average dissipation rate of $\epsilon = 4.92 \times 10^{-8} \text{ W kg}^{-1}$ and is centered on a well-mixed layer (Fig. 3). Although $\bar{\epsilon}$ is only 1/50th of that in the aggregation sampled by MMP 15017, the spectrum is close to the universal form at all wavenumbers.

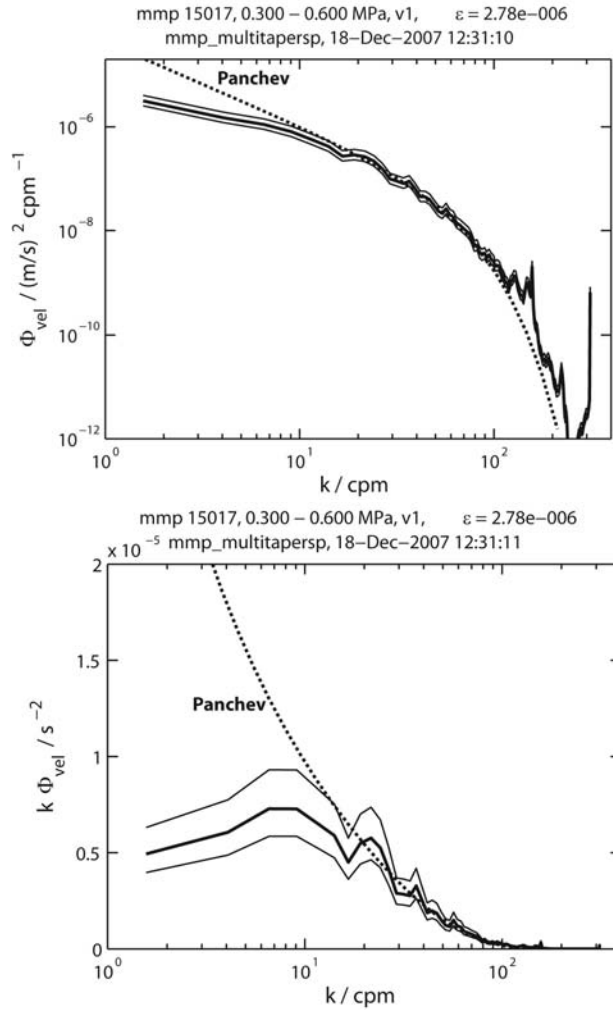


FIG. 10. Velocity spectrum in the fish aggregation sampled by MMP 15017. The spectrum and its variance-preserving form correspond to the shear spectra in Fig. 8. Owing to the low-wavenumber falloff, the variance-preserving form peaks at 8 cpm.

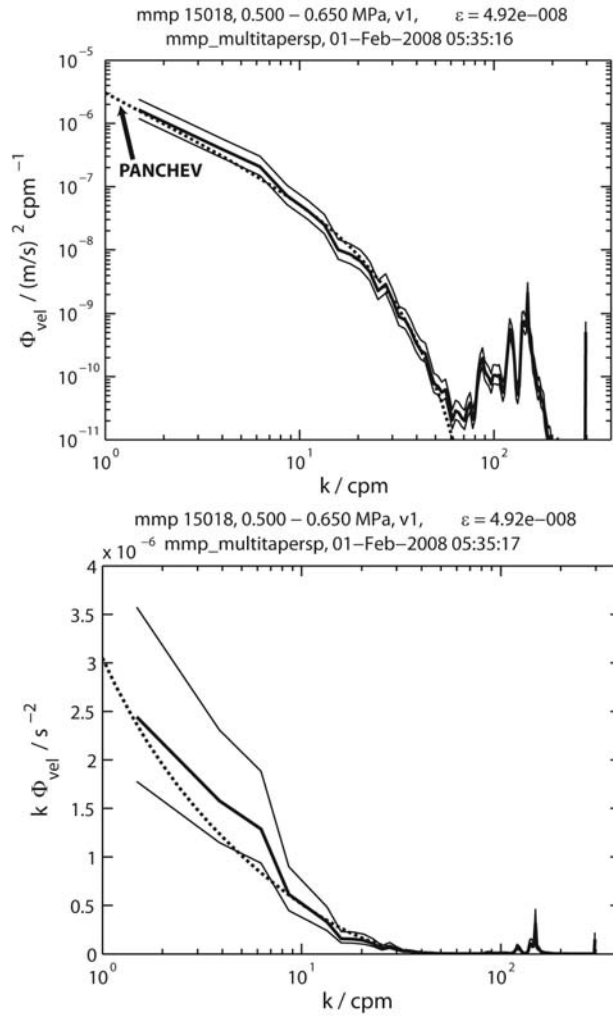


FIG. 11. Average velocity spectrum not in a fish aggregation, corresponding to the MMP 15018 shear spectra in Fig. 9. The spectrum and its variance-preserving form are close to the universal form without peaking at these wavenumbers.

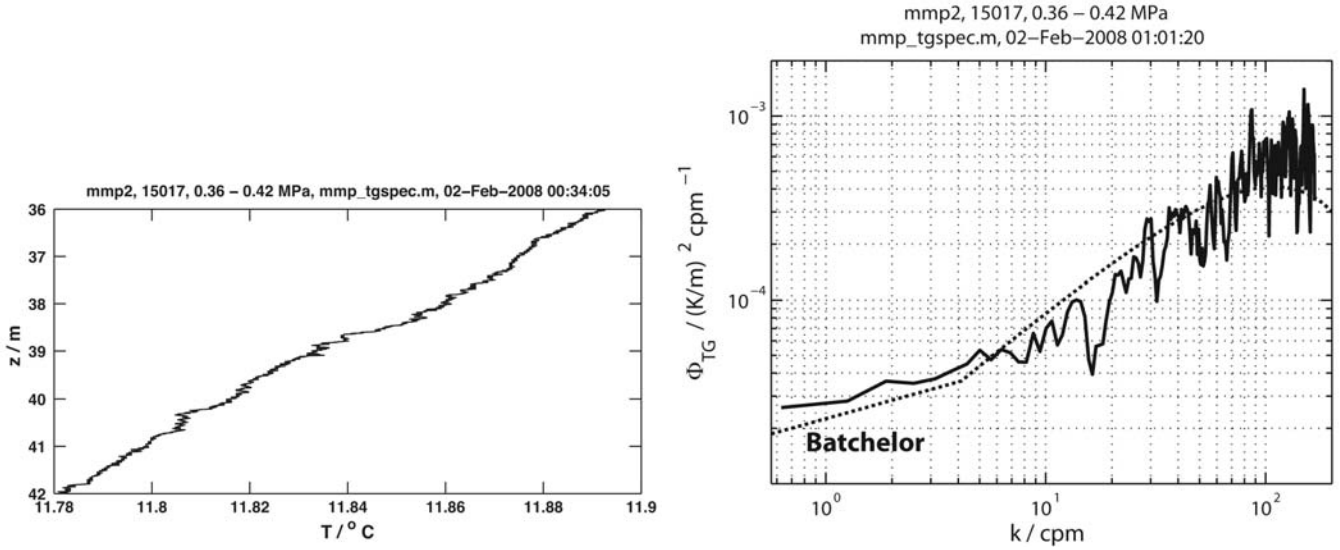


FIG. 12. Left) MMP 15017 FP07 temperature where the mean gradient is nearly linear within the large fish aggregation. Right) The observed temperature gradient spectrum overlaid with a theoretical spectrum consisting of the advective subrange, having a slope of $k^{1/3}$ below 4 cpm, and at higher wavenumbers the Batchelor spectrum for $\epsilon = 2.34 \times 10^{-6} \text{ W kg}^{-1}$. Fitting the Batchelor spectrum to the observed spectrum gave $C = 850$, or $K_T = 1.21 \times 10^{-4} \text{ m}^2 \text{ s}^{-1}$ and $\Gamma = 0.0026$

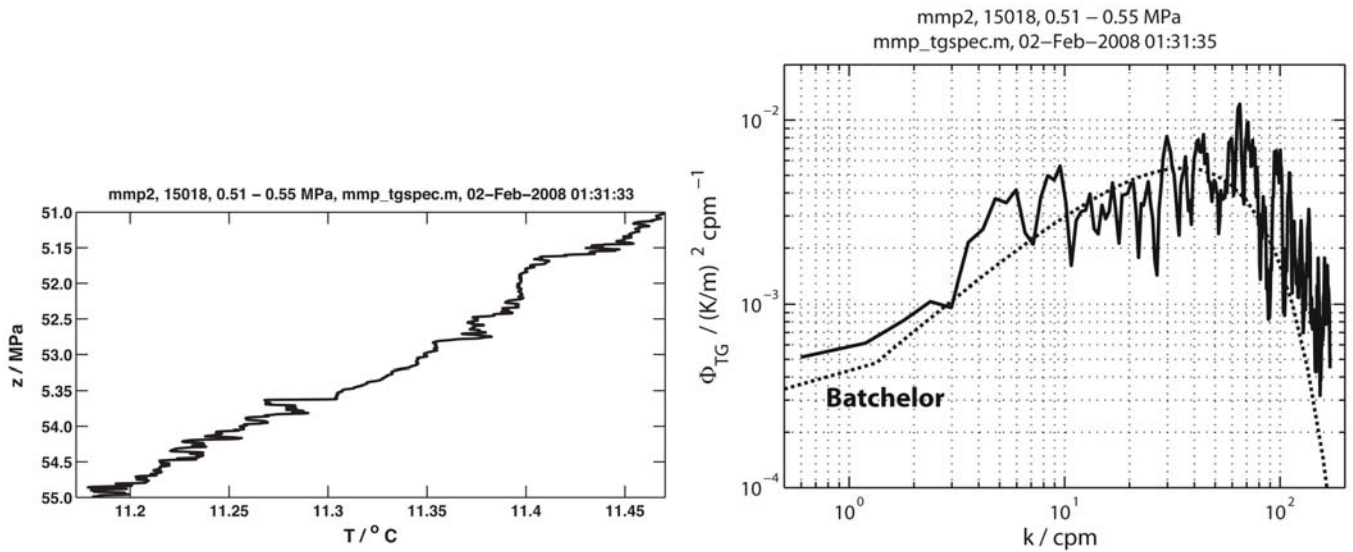


FIG. 13. Left) MMP 15018 FP07 temperature where the mean gradient is nearly linear and not in a fish aggregation. Right) The observed temperature gradient spectrum overlaid with the Batchelor spectrum evaluated with $\epsilon = 2.62 \times 10^{-8} \text{ W kg}^{-1}$. Its fit to the observed spectrum gave $C = 250$, or $K_T = 3.57 \times 10^{-5} \text{ m}^2 \text{ s}^{-1}$ and $\Gamma = 0.203$.

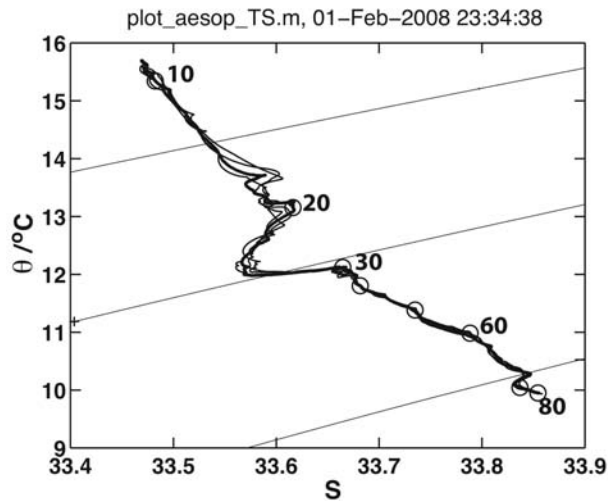


FIG. 14. TS relations of MMP 15017 (thick) and of three nearby profiles (thin). Depth increments of 10 m are marked with circles, some of which are labeled. Linearity between about 30 and 65 m permits estimating overturning scales from temperature.

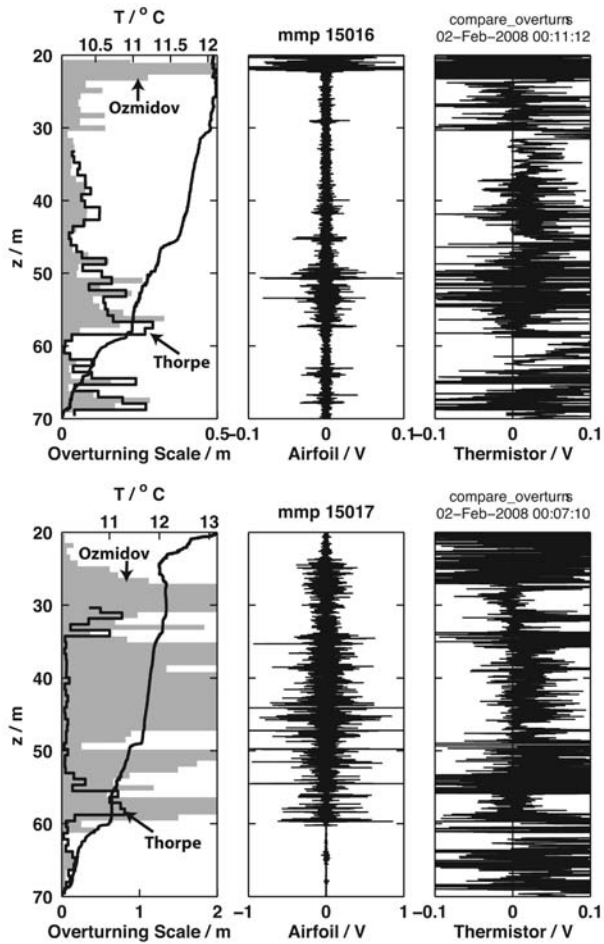


FIG. 15. Left) representative Ozmidov and Thorpe scales outside (MMP 15016) and inside (MMP 15017) aggregations, Middle) bandpassed raw airfoil signals, and Right) raw FPO7 temperature gradient signals. Note that the velocity scale for MMP 15017 is 10 times that of MMP15016, and its overturning scale is four times larger. MMP 15017 started in a low-density shallow extension above the main aggregation, which was between 0.3 and 0.6 MPa. Ozmidov scales greatly exceed Thorpe scales throughout, unlike the situation in MMP 15016, where the good agreement is typical of that found by many investigators.

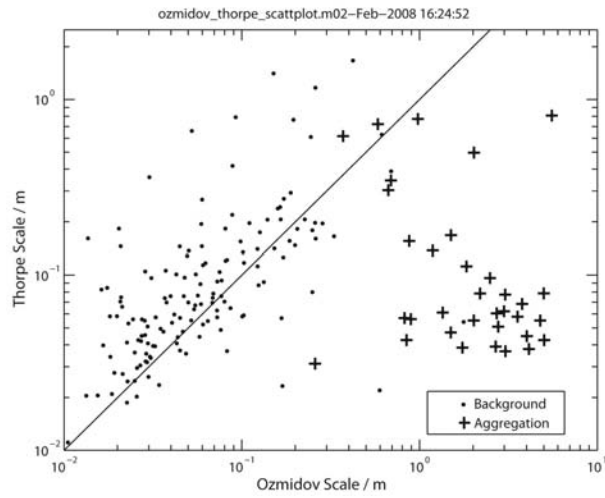


FIG. 16. Scatter plot of Thorpe scales, i.e., observed root-mean-square overturning scales, versus Ozmidov scales, L_{OZ} , for MMP profiles 15015–15018. Within aggregations Thorpe scales are likely to be much smaller than Ozmidov scales.

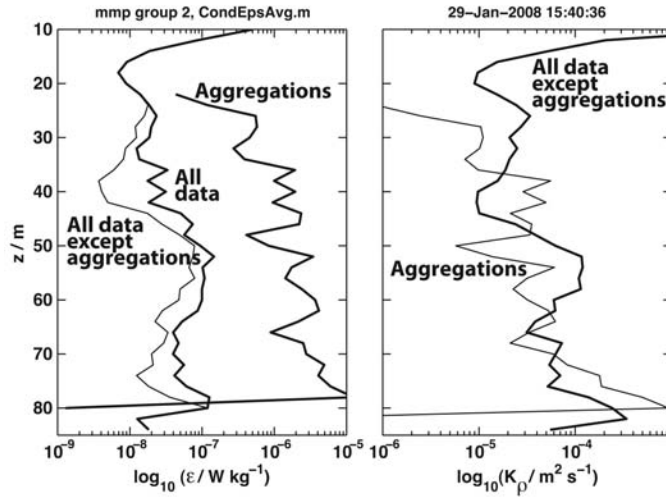


FIG. 17. Left) Averages of a) the 142 dissipation profiles comprising Group 2, b) the three profiles in large, intense fish aggregations, and c) the 139 profiles not in large aggregations. Right) Average K_ρ of the 139 profiles not in large aggregations using $\Gamma = 0.2$ and for the three profiles in aggregations using $\Gamma = 0.0022$, the average efficiency found in aggregations. Although ϵ in aggregations averages 100 times that outside, the lower efficiency compensates, resulting in no significant difference in K_ρ inside and outside of the aggregations.

List of Tables

1	Parameter values used to detect acoustic backscatter aggregations.	58
2	Characteristics of aggregations in Monterey Bay determined from acoustic backscatter assuming that the aggregations are schools of sardines having the characteristics listed in Table 1. The aggregations are designated by the MMP drop that sampled them, except for 15009*, which profile 15009 narrowly missed. Columns contain average properties of the aggregations. Following \overline{S}_v the properties are: height above the bottom, \overline{h} ; depth, \overline{z} ; width, $\overline{\Delta x}$; thickness, $\overline{\Delta z}$; volume, \overline{V} ; and number of anchovies per unit volume, N_f/\overline{V} . Of these eleven profiles, all except 17259 were taken during Group 2.	59
3	Estimates of mixing efficiency, Γ , made by comparing temperature and velocity microstructure in profile sections having nearly uniform temperature gradients. Profile numbers of sections in aggregations are underlined. Γ values in the aggregations were about 1% of those outside aggregations.	60

TABLE 1. Parameter values used to detect acoustic backscatter aggregations.

Parameter	Value
Min. data threshold	65 dB
Max. data threshold	5 dB
Min. total school length	30 m
Min. total school height	10 m
Min. candidate length	5 m
Min. candidate height	2 m
Max. vertical linking distance	5 m
Max. horizontal linking distance	20 m
Distance mode: GPS	

TABLE 2. Characteristics of aggregations in Monterey Bay determined from acoustic backscatter assuming that the aggregations are schools of sardines having the characteristics listed in Table 1. The aggregations are designated by the MMP drop that sampled them, except for 15009*, which profile 15009 narrowly missed. Columns contain average properties of the aggregations. Following $\overline{S_v}$ the properties are: height above the bottom, \bar{h} ; depth, \bar{z} ; width, $\overline{\Delta x}$; thickness, $\overline{\Delta z}$; volume, \bar{V} ; and number of anchovies per unit volume, N_f/\bar{V} . Of these eleven profiles, all except 17259 were taken during Group 2.

MMP	$\overline{S_v}$	\bar{h}	\bar{z}	$\overline{\Delta x}$	$\overline{\Delta z}$	\bar{V}	N_f/\bar{V}
	dB	m	m	m	m	m ³	m ⁻³
15045	-41.5	20.9	66.7	60.2	45.7	2.22×10^4	198×10^1
15009*	-45.5	38.2	53.2	145.6	73.3	1.87×10^5	8.00×10^{-1}
14929	-46.4	9.8	21.1	103.2	21.1	7.75×10^3	6.42×10^{-1}
14934	-47.0	14.6	24.0	71.6	29.1	1.22×10^4	5.59×10^{-1}
15057	-47.1	312	64.2	73.9	52.9	4.82×10^4	5.45×10^{-1}
15017	-48.9	41.4	47.5	189.5	737	2.70×10^5	3.66×10^{-1}
15041	-49.7	22.3	58.9	157.0	62.0	1.70×10^5	304×10^{-1}
15009	-50.1	24.0	64.0	25.8	49.5	8.38×10^3	2.21×10^{-1}
14949	-52.8	6.1	44.5	75.4	23.2	1.93×10^3	1.49×10^{-1}
17259	-53.2	20.3	24.5	138.3	37.0	3.73×10^4	1.37×10^{-1}
14919	-58.4	5.4	73.9	40.8	10.9	9.06×10^2	4.04×10^{-2}
14950	-60.7	8.7	45.7	58.6	28.8	3.00×10^3	8.45×10^{-3}

TABLE 3. Estimates of mixing efficiency, Γ , made by comparing temperature and velocity microstructure in profile sections having nearly uniform temperature gradients. Profile numbers of sections in aggregations are underlined. Γ values in the aggregations were about 1% of those outside aggregations.

Profile	z / m	$\epsilon / \text{W kg}^{-1}$	N^2 / s^{-2}	C	$K_T / \text{m}^2 \text{s}^{-1}$	Γ
15015	47.3-49.8	3.29×10^{-9}	1.11×10^{-4}	40	5.71×10^{-6}	0.197
15015	50.0-53.0	5.14×10^{-8}	1.72×10^{-4}	700	9.98×10^{-5}	0.333
15015	53.1-58.3	1.88×10^{-8}	3.10×10^{-5}	1000	1.43×10^{-4}	0.235
<u>15017</u>	33.7-35.5	1.68×10^{-6}	1.32×10^{-4}	700	1.00×10^{-4}	0.0078
<u>15017</u>	36.0-42.0	2.34×10^{-6}	5.08×10^{-5}	850	1.21×10^{-4}	0.0026
<u>15017</u>	42.0-46.0	4.69×10^{-6}	6.02×10^{-5}	800	1.14×10^{-4}	0.0015
<u>15017</u>	50.0-53.0	7.53×10^{-6}	9.79×10^{-5}	1000	1.43×10^{-4}	0.0019
15018	51.0-55.0	2.61×10^{-8}	1.49×10^{-4}	250	3.57×10^{-5}	0.203
15041	36.0-40.0	1.45×10^{-8}	9.59×10^{-5}	120	1.71×10^{-5}	0.113
<u>15041</u>	55.0-57.0	3.76×10^{-6}	4.28×10^{-5}	1000	1.43×10^{-4}	0.0016
<u>15041</u>	61.6-64.3	3.42×10^{-6}	2.33×10^{-4}	500	7.13×10^{-5}	0.0049
<u>15057</u>	36.0-46.0	3.45×10^{-7}	9.49×10^{-5}	500	7.14×10^{-5}	0.0195
<u>15057</u>	63.6-66.0	9.35×10^{-7}	1.14×10^{-5}	700	9.96×10^{-5}	0.0012
<u>15057</u>	73.0-75.0	4.08×10^{-6}	7.83×10^{-5}	500	7.11×10^{-5}	0.0014